J. Fluid Mech. (1994), *vol.* 278, *pp.* 149–174

Unsteady electrophoretic motion of a non-spherical colloidal particle in an oscillating electric field

By MICHAEL LOEWENBERG†
Department of Physical Chemistry, University of Sydney, NSW, 2006, Australia

(Received 30 August 1993 and in revised form 23 May 1994)

The oscillatory motion of an electrically charged non-spherical colloidal particle in an oscillating electric field is investigated. The particle is immersed in an incompressible viscous fluid and assumed to have a thin electric double layer. For moderate-aspect-ration spheroids and cylinders, a simple algebraic expression is derived that accurately describes oscillatory electrophoretic particle motion in terms of the steady Stokes resistance, added mass, and Basset force. The effects of double-layer conduction and displacement currents within dielectric particles are included. The results indicate that electroacoustic measurements may be able to determine the ζ–potential, dielectric constant, surface conductivity (and microstructural information contained therein), size, density, volume fraction, and possibly shape of non-spherical particles in a dilute suspension. A simple formula is obtained for the high-frequency electrical conductivity of a dilute suspension of colloidal spheroids with arbitrary charge and dielectric constant; only the added mass and Basset force are required and the requisite parameters are given. The result is needed for electroacoustic measurements but it may also be independently useful for determining the dielectric constant, surface conductivity, volume fraction, and possibly the shape of non-spherical particles in a dilute suspension. Electroacoustic energy dissipation is described for a dilute colloidal suspension. It is shown that resistive electrical heating and viscous dissipation occur independently. Electrical and viscous dissipation coefficients that characterize the order volume fraction contributions of the suspended particles are calculated; the electrical dissipation coefficient is $O(1)$ for all oscillation frequencies, whereas the latter vanishes at low- and high-frequencies. The fluid motion is shown to be a superposition of unsteady, viscous and potential flows past an oscillating particle with no applied electric field. The electro-osmotic flow field is insensitive to particle geometry and qualitatively different from the flow past an oscillating particle with no applied field.

1. Introduction

Colloidal particles generally bear a non-zero electric potential (ζ–potential) on their surface, and in a suspending electrolyte, a diffuse electric double layer forms. There is no net electrical charge on the particle and the surrounding double layer; nevertheless, colloidal particles will generally migrate, force-free, through a suspending fluid under the influence of an electric field (Hunter 1987; Russel, Saville & Schowalter 1989). In most applications, the fluid motion is quasi-steady. Recently, electroacoustic devices have been developed for efficiently characterizing colloidal suspensions (O'Brien 1988, 1990; Marlowe, Fairhurst & Pendse 1988); these devices rely on an understanding of unsteady, electrophoretic motion.

† Current address: Department of Applied Mathematics and Theoretical Physics, Cambridge University, Cambridge, CB3 9EW, UK.

When a sound wave travels through a colloidal suspension, a measurable electric field, oscillating at the same frequency as the sound wave, can be generated. This effect arises from the relative motion between the particles and the diffuse portion of their electric double layers resulting from the density difference of the particles and the suspending fluid. This effect was first postulated by Debye (1933) in the context of ion motion in electrolytic solutions. Since that time, there have been several investigations of the phenomenon in colloidal suspensions (Hermans 1938; Enderby 1951; Booth & Enderby 1952). The converse effect, an oscillating electric field produced a sound wave of the same frequency, has been observed but not explained until recently (O'Brien 1988).

For moderate sound wave amplitudes and electric field strengths, the average, microscopic particle velocity in a suspension is linearly related to the average velocity and electric field,

$$\boldsymbol{U}^P = \boldsymbol{M}^0 \cdot \boldsymbol{U}^\infty + \frac{\epsilon\zeta}{\mu} \boldsymbol{M}^E \cdot \boldsymbol{E}^\infty, \tag{1.1}$$

where $\boldsymbol{M}^0$ and $\boldsymbol{M}^E$ are the (dimensionless) unsteady, hydrodynamic and electrophoretic particle mobility tensors. As indicated, $\boldsymbol{M}^E$ is normalized by the Smoluchowski (1903) formula, $\epsilon\zeta/\mu$ that describes quasi-steady electrophoresis of a moderately charged particle with a thin electric double layer, where μ and ϵ are the dynamic viscosity and dielectric constant of the suspending fluid. Brownian motion and sedimentation are neglected in (1.1) because we are interested in unsteady, oscillatory motion that occurs on a timescale of ~ 1 μs, which is short compared to the timescale of diffusive or gravity-driven motion of micron-size particles.

Under quite general conditions, the average current density in a colloidal suspension is (O'Brien 1990)

$$\boldsymbol{J}^\infty = \boldsymbol{K}^* \cdot \boldsymbol{E}^\infty + c\frac{\epsilon\zeta}{\mu}(\Delta\rho_P/\rho)\boldsymbol{M}^E \cdot \nabla P^\infty, \tag{1.2}$$

where $\boldsymbol{K}^*$ is the unsteady, electrical conductivity tensor of the suspension; c and $\Delta\rho_P = \rho_P - \rho$ are the volume fraction and excess density of the suspended particles. Both $\boldsymbol{K}^*$ and $\boldsymbol{M}^E$ depend on microscopic properties of the suspended particles; however, $\boldsymbol{K}^*$ may often be conveniently determined by independent measurements ($\nabla P^\infty = 0$) (Russel *et al.* 1989) so that it may be considered a known parameter in (1.2). Thus, macroscopically measurable pressure, voltage, and current are linked to microscopic suspension parameters via $\boldsymbol{M}^E$. This is the basis of electroacoustic devices that have recently been developed for rapid reliable characterization of colloidal suspensions. Unfortunately, the unsteady, electrophoretic mobility is known only for suspensions of spherical particles (O'Brien 1988; Mangelsdorf & White 1992; Sawatzky & Babchin 1993; Rider & O'Brien 1993). The only exception is for dilute suspensions of spheroidal particles with thin electrical double layers and moderate surface charge (Loewenberg & O'Brien 1992). The aim of this paper is to investigate the unsteady electrophoretic motion of a non-spherical, colloidal particle with special attention to the effects of particle shape, charge, and dielectric constant.

The problem is formulated and assumptions are stated in §2. The unsteady electro-osmotic flow past a charged colloidal particle in an oscillating electric field is derived and illustrated in §3. Detailed aspects of unsteady viscous flows are significant because of their impact on microscale heat and mass transport during electroacoustic measurements. An 'electro-osmotic resistance' is determined that relates the electric field strength to the force acting on a charged stationary particle; the results are used to determine electrophoretic particle motion. In §§4 and 5, earlier results for the

electrophoretic mobility of moderately charged spheroids with thin electric double layers (Loewenberg & O'Brien 1992) are extended to include highly charged and cylindrical particles. According to (1.2), electroacoustic measurements also require knowledge of the suspension conductivity; fortuitously, a simple formula for the high-frequency electrical conductivity by a dilute suspension of colloidal spheroids with arbitrary charge and dielectric constant is obtained as a bi-product of the analysis. Energy dissipation adversely affects the performance of electroacoustic devices; in §6, electroacoustic energy dissipation is described for a dilute suspension of non-spherical particles. Concluding remarks are made in §7. Throughout the article, the effects of particle shape, charge, and dielectric constant are highlighted. According to relation (1.2) the results of this work will strengthen the link between macroscopically measurable pressure, voltage, and current and microscopic suspension parameters. Furthermore, this work should advance the present understanding of microscopic unsteady viscous flows.

2. Problem formulation and assumptions

2.1. *Electric field*

The applied oscillating electric field is described by $\boldsymbol{E}^{\infty}\cos\omega t$. In this paper, $c \ll 1$ is assumed; accordingly, $\boldsymbol{E}(\boldsymbol{x},t)\to\boldsymbol{E}^{\infty}\cos\omega t$ far from the particle. Henceforth, the electric field is normalized by $\boldsymbol{E}^{\infty}$. For electroacoustic applications, high oscillation frequencies, greater than 1 KHz but less than 10^3 MHz, are of particular interest. Herein, $10^3 \ll \omega \ll 10^9$ rad s^{-1} is assumed; for ω in this range, electrophoretic motion is unsteady, and high-frequency electrical dispersion occurs. The wavelength of electromagnetic radiation is very large compared to the particle size so that Maxwell's equations reduce to the quasi-steady (electrostatic) form (Jackson 1962):

$$\nabla\cdot\boldsymbol{E}(\boldsymbol{x}) = 0, \quad \nabla\times\boldsymbol{E}(\boldsymbol{x}) = 0, \tag{2.1}$$

where $\boldsymbol{E}(\boldsymbol{x},t) = \boldsymbol{E}(\boldsymbol{x})\,e^{-i\omega t}$ has been assumed; by the linearity of (2.1)–(2.3), general time-dependent behaviour can be constructed from the Fourier components of $\boldsymbol{E}(\boldsymbol{x},t)$.

The electric double-layer thickness, given by the Debye length, κ^{-1}, is small compared to the particle size in many applications. For example, $\kappa a \sim 10^3 az(10m)^{1/2}$, in an m molar, z-valent, symmetric electrolyte at room temperature, where a is the particle size in microns; thus, $\kappa a \gg 1$ except for very weak electrolytes or particles much smaller than micron-size. Herein, $\kappa a \gg 1$ is assumed, where a is the minimum particle dimension. For thin electric double layers and frequencies in the assumed range, the boundary condition for the electric field on the particle surface is (Dukhin & Derjaguin 1974; O'Brien 1983, 1986)

$$(1+\lambda_E^2)\,\boldsymbol{E}\cdot\boldsymbol{n} - \lambda_E^2(\epsilon_P/\epsilon)\,\hat{\boldsymbol{E}}\cdot\boldsymbol{n} = -\tilde{K}^S\nabla_S\cdot\boldsymbol{E}, \tag{2.2}$$

where $\hat{\boldsymbol{E}}$ is the intraparticle field, $\boldsymbol{n}$ is the outward normal on the particle surface, ∇_S is the surface gradient operator, $\lambda_E = (\epsilon\omega/K^{\infty})^{1/2}e^{-i\pi/4}$ is a complex-valued electrical frequency parameter, $\tilde{K}^S = K^S/aK^{\infty}$ is the dimensionless surface conductivity of the particle, discussed below, and ϵ_P is the dielectric constant of the particle. Apparently, the particle behaves as a conductor if $\lambda_E^2\epsilon_P/\epsilon \neq 0$ or $\tilde{K}^S \neq 0$. The tangential portion of the electric field, $\boldsymbol{E}_t$, is continuous across the particle surface:

$$\boldsymbol{E}_t = \hat{\boldsymbol{E}}_t, \tag{2.3}$$

which completes the specification of the electric field.

The suspending fluid (electrolyte) has the complex-valued isotropic conductivity

$K = K^\infty - i\omega\epsilon$ that incorporates the contribution, K^∞, from the migration of charged species and the displacement current associated with the dielectric constant of the fluid (Russel *et al.* 1989). Thus, $|\lambda_E|^2$ is the ratio of the dielectric relaxation time for the fluid to the period of electric field oscillation; typically, $K^\infty/\epsilon \sim 1$ MHz. According to boundary condition (2.2), the electric field is independent of λ_E for non-conducting particles ($\epsilon_P/\epsilon = \tilde{K}^S = 0$). The particle conductivity is $-i\omega\epsilon_P$; only displacement currents pass through its interior. The dielectric constant of water is very large, about 80 times the permittivity of a vacuum, thus ϵ_P/ϵ is usually small; however, important exceptions exist: for example $\epsilon_P/\epsilon \approx 1$ for TiO_2 and some hydrocarbons (Russel *et al.* 1989; Harnwell 1949, p. 88). Typically, $ze\zeta/kT = O(1)$, where $kT/e = 25.4$ mV (e is the charge on an electron, k is the Boltzmann constant, and T is absolute temperature). A highly charged particle, $ze\zeta/kT \gg 1$, is endowed with an additional surface conductivity (Dukhin & Derjaguin 1974; O'Brien 1983, 1986): $\tilde{K}^S \approx \exp(|ze\zeta|/2kT)/\kappa a$; for example, $\tilde{K}^S \approx 1$ for $\zeta = 150$ mV, $\kappa a = 50$. Physically, surface conductivity arises from the high density of mobile counterions in the thin diffuse portion of the electric double layer; the charge density in this layer depends exponentially on the surface charge.

2.2. *Fluid velocity*

A complex-valued viscous frequency parameter, $\lambda = a(\omega/\nu)^{1/2} e^{-i\pi/4} = a(K^\infty/\epsilon\nu)^{1/2}\lambda_E$, characterizes the fluid motion where ν is the kinematic viscosity of the suspending fluid, and λ_E is the electrical frequency parameter defined above; $|\lambda|^2$ is the ratio of the viscous relaxation time to the period of the electric field. Assuming $K^\infty/\epsilon \sim 1$ MHz (Russel *et al.* 1989), $|\lambda| \sim a|\lambda_E|$ in water, where a is the particle size in microns, and $|\lambda| = |\lambda_E| = 1$ for a 1 μm particle (in water) with $\omega = 10^6$ rad s^{-1}.

In general, the Navier–Stokes equations govern the fluid motion. Boundary condition (2.5) suggests that the characteristic electro-osmotic fluid velocity is $U_C = E^\infty\epsilon\zeta/\mu$ for fluid motion driven by an applied electric field, which is the Smoluchowski formula for quasi-steady electrophoresis of a moderately charged particle with a thin electric double layer; the characteristic displacement of the oscillating fluid is U_C/ω. In most situations of interest, the fluid displacement is very small compared to particle size, $U_C/\omega a \ll 1$. Typically, $\epsilon\zeta/\mu \sim 10^{-4}$ cm^2 V^{-1} s^{-1} and $E^\infty \sim 10$ V cm^{-1} yielding, $U_C = 10^{-3}$ cm s^{-1}, and $U_C/\omega a \sim 10^{-5}$ for a micron-size particle at the typical frequency for electroacoustic measurements, $\omega \sim 10^6$ rad s^{-1}.

According to the above estimates, the Reynolds number based on particle size is small: $Re = U_C a/\nu = (U_C/\omega a)|\lambda|^2 \ll 1$. The fluid may be considered locally incompressible if the wavelength of sound is large compared to the particle size at the oscillation frequency, ω (Batchelor 1967). This is generally true at the frequencies of interest; for example, the wavelength of sound in water is 1 cm at the typical frequency $\omega \sim 10^6$ rad s^{-1}. Thus, the unsteady Stokes equations govern the fluid velocity and pressure (Kim & Karrila 1991):

$$\nabla^2\boldsymbol{u}(\boldsymbol{x}) - \nabla p(\boldsymbol{x}) = \lambda^2\boldsymbol{u}(\boldsymbol{x}), \quad \nabla\cdot\boldsymbol{u}(\boldsymbol{x}) = 0, \tag{2.4}$$

where $\boldsymbol{u}(\boldsymbol{x}, t) = \boldsymbol{u}(\boldsymbol{x})e^{-i\omega t}$ has been assumed; general time-dependent behaviour can be constructed from the Fourier components of $\boldsymbol{u}(\boldsymbol{x}, t)$ because of the linearity of (2.1)–(2.5) (Basset 1888; Lawrence & Weinbaum 1988). The unsteady Stokes equations have been non-dimensionalized using a characteristic velocity and pressure, U_C and $\mu U_C/a$, where U_C depends on the relevant boundary conditions as discussed below. By the assumed diluteness and incompressibility of the suspension, $\boldsymbol{u}(\boldsymbol{x}, t)$ tends to the uniform oscillating field, $\boldsymbol{U}^\infty \cos\omega t$, far from the particle.

For thin electric double layers, the fluid velocity satisfies the electro-osmotic 'slip'

boundary condition on the particle surface (Dukhin & Derjaguin 1974; O'Brien 1983, 1986):

$$\boldsymbol{u} = \frac{\boldsymbol{U}^P}{U_C} - \frac{\boldsymbol{E}^\infty}{U_C}\frac{\epsilon\zeta}{\mu}\boldsymbol{E}_t, \tag{2.5}$$

which couples the fluid velocity to the electric field. The mobile, or diffuse, portion of the double layer contains a net charge equal and opposite to that on the particle surface; the electro-osmotic slip velocity arises from the convection of this electrically charged fluid layer by the electrical body force. The charge density, and thus the body force, vanish outside the thin double layer. Boundary condition (2.5) is derived using a quasi-steady description of the flow field within the electric double layer; thus, the double layer is assumed to be much thinner than the viscous boundary layer, $\kappa a \gg |\lambda| + 1$.

3. Unsteady electro-osmotic flow; non-conducting particles

3.1. *Unsteady electro-osmotic flow field*

For $\boldsymbol{U}^\infty = \boldsymbol{E}^\infty = 0$, equations (2.4) and (2.5) describe the unsteady, velocity field, $\boldsymbol{u}^0(\boldsymbol{x})$, past a particle oscillating with the prescribed velocity, $\boldsymbol{U}^P \cos\omega t$, in a quiescent fluid without an applied electric field. In this case, $U_C = U^P$ so that (2.5) reduces to the no-slip boundary condition $\boldsymbol{u}^0(\boldsymbol{x}) = \boldsymbol{e}$ on the particle surface, where $\boldsymbol{e}$ is a unit vector parallel to $\boldsymbol{U}^P$. For $\boldsymbol{U}^P = \boldsymbol{E}^\infty = 0$, (2.4) and (2.5) describe the unsteady velocity field past a stationary particle in an oscillating ambient fluid, $\boldsymbol{U}^\infty \cos\omega t$; the (dimensional) velocity field in this case is simply $\boldsymbol{U}^\infty[\boldsymbol{e} - \boldsymbol{u}^0(\boldsymbol{x})]$. For $\boldsymbol{U}^\infty = \boldsymbol{U}^P = 0$, (2.4) and (2.5) describe the unsteady electro-osmotic flow field, $\boldsymbol{u}^E(\boldsymbol{x})$, past a stationary electrically charged particle in an oscillating electric field, $\boldsymbol{E}^\infty \cos\omega t$. By taking $U_C = E^\infty \epsilon\zeta/\mu$, (2.5) reduces to $\boldsymbol{u}^E(\boldsymbol{x}) = -\boldsymbol{E}_t$; the electro-osmotic velocity field is electrically driven by the slip velocity on the particle surface. The total velocity field in a dilute suspension is given by a superposition of the velocity fields discussed above:

$$\boldsymbol{u}(\boldsymbol{x}) - \boldsymbol{U}^\infty = (\boldsymbol{U}^P - \boldsymbol{U}^\infty)\,\boldsymbol{u}^0(\boldsymbol{x}) + \frac{\epsilon\zeta}{\mu}\boldsymbol{E}^\infty \boldsymbol{u}^E(\boldsymbol{x}). \tag{3.1}$$

Kinematical features of unsteady viscous flows are important for understanding convective heat and mass transport processes between particles and the suspending fluid that may occur during electroacoustic measurements (Ghaddar *et al.* 1986; Sobey 1985). The unsteady viscous flow field $\boldsymbol{u}^0(\boldsymbol{x})$ has been the subject of several studies (e.g. Pozrikidis 1989*a*; Loewenberg 1994*a*, *b*). For the remainder of this section, we focus on the unsteady electro-osmotic velocity field, $\boldsymbol{u}^E(\boldsymbol{x})$, which has not been previously investigated.

For non-conducting particles ($\epsilon_P/\epsilon = \tilde{K}^S = 0$) the normalized electric field is quasi-steady and can be expressed as

$$\boldsymbol{E}(\boldsymbol{x}) = \boldsymbol{e} - \boldsymbol{u}^P(\boldsymbol{x}), \tag{3.2}$$

where $\boldsymbol{e}$ is parallel to the applied field, and $\boldsymbol{u}^P(\boldsymbol{x})$ is the linearized potential flow field that satisfies (2.1), vanishes at infinity, and $\boldsymbol{u}^P \cdot \boldsymbol{n} = \boldsymbol{e} \cdot \boldsymbol{n}$, on the particle surface; $\boldsymbol{u}^P(\boldsymbol{x})$ is the high-frequency potential-flow limit of $\boldsymbol{u}^0(\boldsymbol{x})$ that is valid for points outside of the $|\lambda|^{-1}$ boundary layer on the particle surface (Batchelor 1967). Thus, (3.2) satisfies (2.1), tends to $\boldsymbol{e}$ at infinity, and satisfies $\boldsymbol{E}(\boldsymbol{x}) \cdot \boldsymbol{n} = 0$ on the particle surface, as required. The unsteady electro-osmotic velocity field past a stationary non-conducting particle in an oscillating electric field is given by

$$\boldsymbol{u}^E(\boldsymbol{x}) = \boldsymbol{e} - \boldsymbol{u}^0(\boldsymbol{x}) - \boldsymbol{E}(\boldsymbol{x}), \tag{3.3}$$

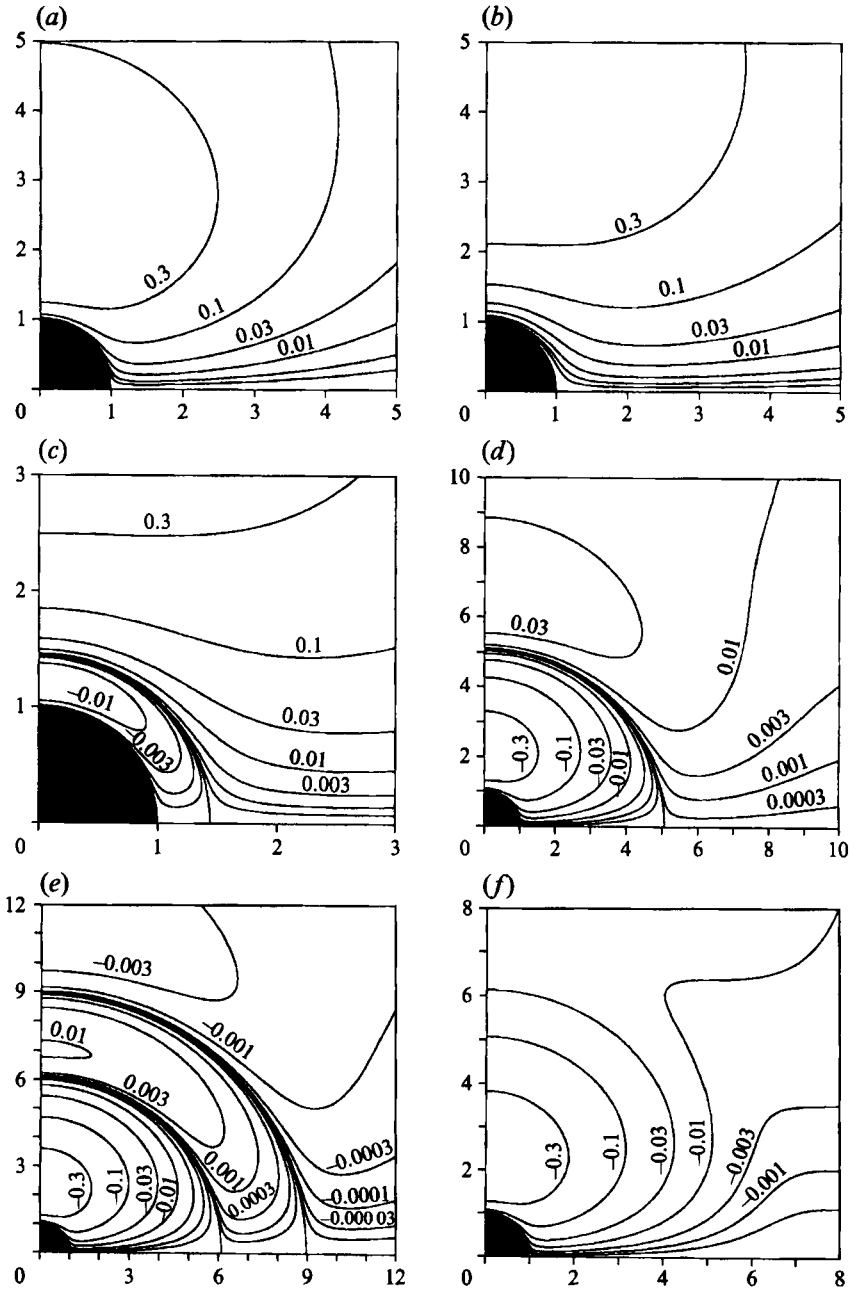

FIGURE 1. Instantaneous streamlines for unsteady electro-osmotic flow past a non-conducting sphere with $|\lambda| = 1$. Streamfunction values follow the sequence: $\phi = 0.3, 0.1, 0.03, 0.01, \ldots, 0, \ldots, -0.01, -0.03, -0.1, -0.3$; streamlines are labelled accordingly where space permits. (*a*) $\omega t = 0$, (*b*) 0.50π, (*c*) 0.55π, (*d*) 0.85π, (*e*) 0.88π, (*f*) 0.90π.

where $\boldsymbol{e}$ is parallel to $\boldsymbol{E}^{\infty}$, and $\boldsymbol{u}^0(\boldsymbol{x})$ is the unsteady viscous flow field defined above (3.1). The expression vanishes at infinity and satisfies the unsteady Stokes equations because solutions of (2.1) also satisfy (2.4). On the surface of a non-conducting particle, $\boldsymbol{E}_t \equiv \boldsymbol{E}$; thus, (3.3) satisfies boundary condition (2.5) for electro-osmotic flow

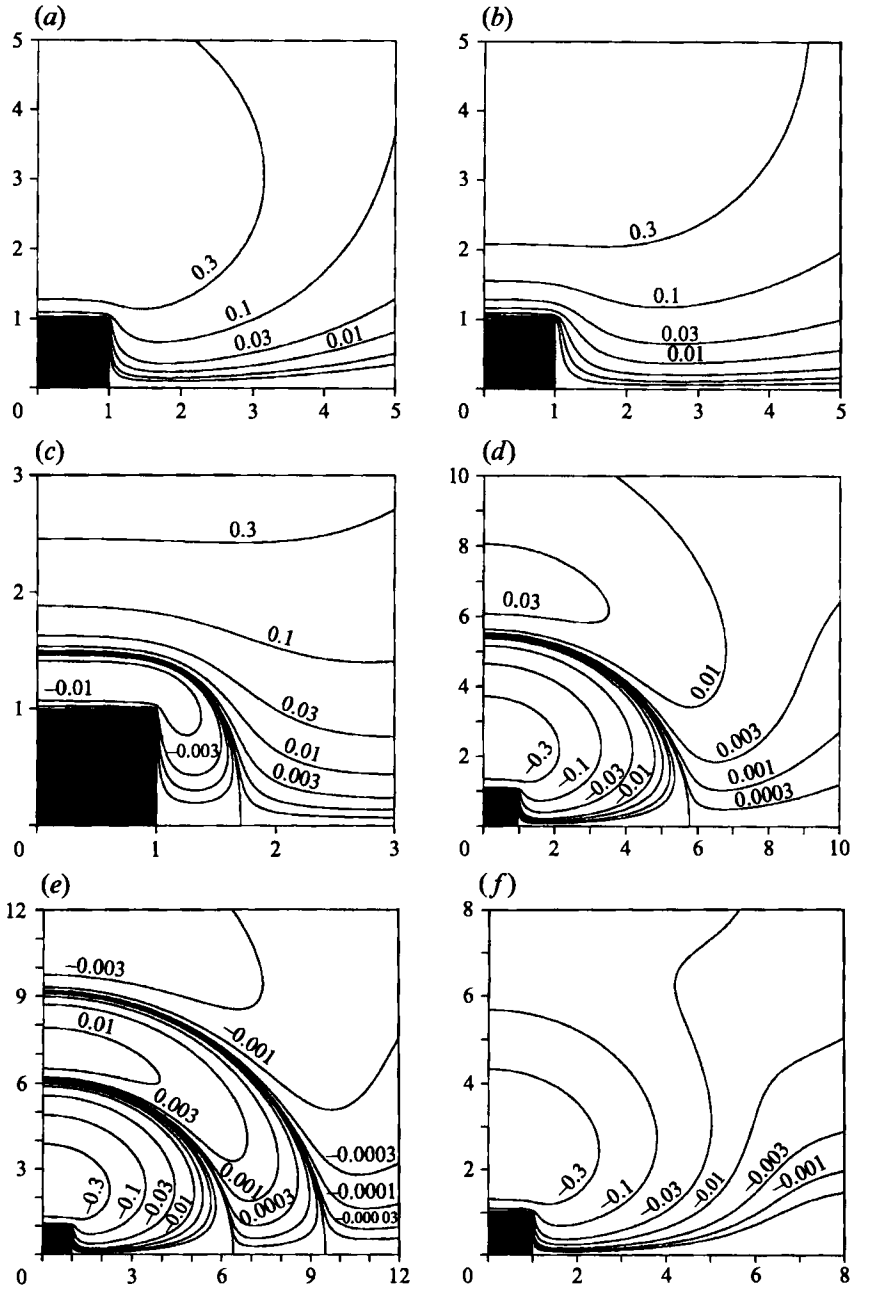

FIGURE 2. Instantaneous streamlines for unsteady electro-osmotic flow past a non-conducting unit-aspect-ratio cylinder with $|\lambda| = 1$. Streamfunction values as for figure 1. (*a*) $\omega t = 0$, (*b*) 0.50π, (*c*) 0.55π, (*d*) 0.85π, (*e*) 0.865π, (*f*) 0.90π.

($\boldsymbol{U}^{\infty} = \boldsymbol{U}^{P} = 0$). Substituting (3.2) into (3.3) yields the simple superposition solution for the unsteady electro-osmotic velocity field past any non-conducting particle:

$$\boldsymbol{u}^{E}(\boldsymbol{x}) = \boldsymbol{u}^{P}(\boldsymbol{x}) - \boldsymbol{u}^{0}(\boldsymbol{x}). \tag{3.4}$$

The sequence of instantaneous streamline patterns in figures 1 and 2 depict unsteady electro-osmotic flow past a stationary non-conducting particle in an oscillating field

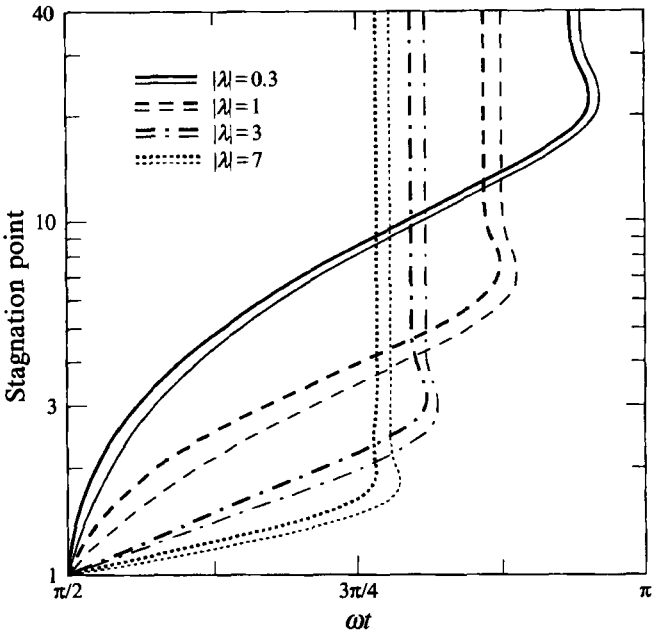

FIGURE 3. Instantaneous size of recirculating eddy, depicted by the location of the forward stagnation point (cf. figures 1 and 2), for unsteady electro-osmotic flow past a non-conducting sphere (thinner curves) and unit-aspect-ratio cylinder (thicker curves).

with $|\lambda| = 1$. For a sphere (figure 1), the results were obtained analytically by inserting Stokes's (1851) solution into (3.4). For other particle shapes, results can be obtained by superposition of numerical solutions according to (3.4); the axisymmetric flow past a unit-aspect-ratio cylinder (diameter = height), depicted in figure 2, was obtained using the calculations of Loewenberg (1994*a*). Recalling the $e^{-i\omega t}$ time dependence and quasi-steady description of the electric field, we conclude that the electrically driven slip velocity on the particle surface is maximal when $\omega t = n\pi$ ($n = 0, 1, 2, \ldots$) and vanishes when $\omega t = (n+\frac{1}{2})\pi$. The unsteady flow field decelerates in a delayed response to the decreasing field strength ($n\pi \leqslant \omega t \leqslant [n+\frac{1}{2}]\pi$); the flow pattern corresponding to $\omega t = (n+\frac{1}{2})\pi$ (figures 1*b*, 2*b*) results from the fluid inertia, and manifests flow field unsteadiness.

Surface flow reversal initiates unsteady flow field reversal. For $\boldsymbol{u}^0(\boldsymbol{x})$, surface flow reversal occurs when the tangential stress distribution changes sign on the particle surface during decelerating portions of the particle oscillation cycle (Pozrikidis 1989*a*; Loewenberg 1994*a*, *b*). An attached recirculating eddy is formed that expands until it encloses the entire particle, continues to expand into the flow field as the particle decelerates further, and it expands to infinity as $(n+\frac{1}{2})\pi - \omega t \to 0$, terminating the flow reversal process. Details of the surface flow reversal and subsequent near-field flow reversal process are sensitive to the detailed particle geometry (Pozrikidis 1989*a*; Loewenberg 1994*a*, *b*).

By contrast, surface flow reversal for unsteady electro-osmotic flow occurs precisely as the applied electric field changes sign. A recirculating eddy, enclosing the entire particle, is instantaneously formed that expands as the applied field strength increases, as illustrated in figures 1(*c*, *d*) and 2(*c*, *d*); forward and rear stagnation points are apparent. An analysis of the far-field velocity indicates that electro-osmotic flow reversal terminates as an exponentially decaying sequence of concentric counter-

rotating eddies annihilate each other during the interval $(n+\frac{3}{4})\pi \leqslant \omega t \leqslant (n+1)\pi$, as illustrated in figures 1(*e*, *f*) and 2(*e*, *f*); electro-osmotic flow reversal terminates earlier at higher frequencies, later for lower. The evolution of the recirculating eddy is depicted in figure 3 for several oscillation frequencies; the over-shooting oscillatory behaviour illustrates the predicted occurrence of adjacent reversed-flow regions just prior to the termination of flow field reversal. The results depicted in figures 1–3 indicate that unsteady electro-osmotic flow reversal is insensitive to detailed particle geometry, perhaps because electro-osmotic surface flow reversal is the same for all non-conducting particles. Pathlines for all small-amplitude oscillatory flows are elliptical closed orbits (Pozrikidis 1992; Loewenberg 1994*a*).

3.2. *Unsteady electro-osmotic force*

A microscopic particle executing small-amplitude oscillations in a viscous fluid experiences an opposing force: $\boldsymbol{F}^0 = -\mu a \boldsymbol{R}^0 \cdot \boldsymbol{U}^P$, where $\boldsymbol{R}^0$ is the symmetric unsteady viscous resistance tensor. Recalling that $U_C = E^\infty \epsilon\zeta/\mu$ characterizes the electro-osmotic flow field, the unsteady electro-osmotic force that acts on a stationary electrically charged non-conducting particle in an oscillating electric field is obtained from the superposition (3.4): $\boldsymbol{F}^E = \epsilon\zeta a \boldsymbol{R}^E \cdot \boldsymbol{E}^\infty$, where

$$\boldsymbol{R}^E = \boldsymbol{R}^0 - \lambda^2 \boldsymbol{M}^A \tag{3.5}$$

defines the symmetric electro-osmotic resistance tensor and $\boldsymbol{M}^A$ is the added-mass tensor associated with the potential flow field, $\boldsymbol{u}^P(\boldsymbol{x})$.

For spheroids (Lawrence & Weinbaum 1988; Pozrikidis 1989*b*) and finite-length cylinders (Loewenberg 1993*a*), with aspect ratios $1/10 \leqslant \phi \leqslant 10$ (ϕ = length/width),

$$\boldsymbol{R}^0 \approx \boldsymbol{R}^S + \lambda \boldsymbol{B}^\infty + \lambda^2 \boldsymbol{M}^A + \frac{\lambda}{\lambda+1}\left[\frac{1}{6\pi}(\boldsymbol{R}^S \cdot \boldsymbol{R}^S) - \boldsymbol{B}^\infty\right], \tag{3.6}$$

and by (3.5), it follows that

$$\boldsymbol{R}^E \approx \boldsymbol{R}^S + \lambda \boldsymbol{B}^\infty + \frac{\lambda}{\lambda+1}\left[\frac{1}{6\pi}(\boldsymbol{R}^S \cdot \boldsymbol{R}^S) - \boldsymbol{B}^\infty\right], \tag{3.7}$$

where λ is defined by the smallest overall particle dimension perpendicular to its orientation, $\boldsymbol{R}^S$ is the steady Stokes resistance tensor, and

$$\boldsymbol{B}^\infty = \boldsymbol{e}\boldsymbol{e} \int_{S_P} \boldsymbol{u}'(\boldsymbol{x}) \cdot \boldsymbol{u}'(\boldsymbol{x})\, \mathrm{d}S$$

is the Basset force tensor, obtained from the potential flow solution by considering viscous dissipation in the boundary layer (Batchelor 1967), where $\boldsymbol{u}' = \boldsymbol{u}^P - \boldsymbol{e}$ is the potential-flow slip velocity on the particle surface. Exact formulae and numerical results for $\boldsymbol{R}^S$, $\boldsymbol{B}^\infty$, and $\boldsymbol{M}^A$ are available for spheroids and finite-length cylinders (e.g. Loewenberg 1993*a*, *b*). The results (3.6) and (3.7) have the same absolute error and $\approx 5\%$ maximum relative error, attained at $|\lambda| \sim 1$.

Rigorous asymptotic results

$$\boldsymbol{R}^0 = \boldsymbol{R}^S + \frac{\lambda}{6\pi}\boldsymbol{R}^S \cdot \boldsymbol{R}^S + O(\lambda^2), \quad |\lambda| \ll 1; \tag{3.8a}$$

$$\boldsymbol{R}^0 = \lambda^2 \boldsymbol{M}^A + \lambda \boldsymbol{B}^\infty + O(1), \quad |\lambda| \gg 1, \tag{3.8b}$$

are recovered from (3.6) in the appropriate limits. Apparently, $\boldsymbol{R}^E = \boldsymbol{R}^0$ for $|\lambda| \ll 1$

whereas, $\boldsymbol{R}^E = \lambda \boldsymbol{B}^\infty + O(1)$, for $|\lambda| \gg 1$. The distinct high-frequency behaviour is because of the dominant added-mass contribution to $\boldsymbol{R}^0$ that arises from the acceleration of displaced fluid around an oscillating particle; this contribution is absent for a stationary particle with an electrically driven surface velocity. At high frequencies, the electro-osmotic resistance is dominated by viscous dissipation within the $|\lambda|^{-1}$ boundary layer.

4. Unsteady electrophoretic motion; non-conducting particles

Under the assumptions set out in the introduction, the particle motion is force-free and determined by equating the time derivative of particle inertia to the total hydrodynamic resistance resulting from the combined velocity field, (3.1):

$$\lambda^2(\rho_P/\rho)\, V_P\, \boldsymbol{U}^P = \lambda^2 V_P\, \boldsymbol{U}^\infty - (\boldsymbol{U}^P - \boldsymbol{U}^\infty)\cdot \boldsymbol{R}^0 + \frac{\epsilon\zeta}{\mu} \boldsymbol{E}^\infty \cdot \boldsymbol{R}^E, \tag{4.1}$$

where V_P is the (dimensionless) particle volume, and $\lambda^2 V_P\, \boldsymbol{U}^\infty$ is the buoyancy force associated with an oscillating ambient velocity field; $\boldsymbol{R}^0$ and $\boldsymbol{R}^E$ are the resistance tensors defined in §3. Electrically induced rotary particle motion is discussed at the end of this section. The combined velocity field can be obtained by inserting (3.4), (3.5), and (4.1) into (3.1):

$$\boldsymbol{u}(\boldsymbol{x}) - \boldsymbol{U}^\infty = \boldsymbol{U}^\infty \lambda^2 \frac{(-\Delta\rho_P/\rho)\, V_P}{R^0_\alpha + \lambda^2(\rho_P/\rho)\, V_P} \boldsymbol{u}^0(\boldsymbol{x}) + \frac{\epsilon\zeta}{\mu} \boldsymbol{E}^\infty \left[\boldsymbol{u}^P(\boldsymbol{x}) - \lambda^2 \frac{(\rho_P/\rho)\, V_P + M^A_\alpha}{R^0_\alpha + \lambda^2(\rho_P/\rho)\, V_P} \boldsymbol{u}^0(\boldsymbol{x}) \right], \tag{4.2}$$

where R^0_α denotes a principal value of $\boldsymbol{R}^0$; for spheroids and finite-length cylinders, which are explicitly considered, $\alpha = \parallel$ or $\perp$, corresponding respectively to parallel or perpendicular orientation of the particle symmetry axis. By (3.8), the net velocity field for the unsteady force-free motion is irrotational in the quasi-steady low- and high-frequency limits, but not for $|\lambda| = O(1)$.

Incorporating (1.1) and (3.5), (4.1) is inverted to yield the principal values of the unsteady hydrodynamic and electrophoretic particle mobilities in a dilute suspension:

$$M^0_\alpha = \frac{R^0_\alpha + \lambda^2 V_P}{R^0_\alpha + \lambda^2(\rho_P/\rho)\, V_P}; \quad M^E_\alpha = \frac{R^0_\alpha - \lambda^2 M^A_\alpha}{R^0_\alpha + \lambda^2(\rho_P/\rho)\, V_P}. \tag{4.3a, b}$$

For $|\lambda| \to 0$, $M^0_\alpha = 1$. For $|\lambda| > 0$, $|M^0_\alpha| < 1$, $|M^0_\alpha| > 1$, or $M^0_\alpha = 1$ depending on whether $\rho_P/\rho > 1$, $\rho_P/\rho < 1$, or $\rho_P/\rho = 1$. Inserting (3.8b) into (4.3), indicates that $M^0_\alpha = (M^A_\alpha + V_P)/(M^A_\alpha + (\rho_P/\rho)\, V_P)$ in the high-frequency limit. Smoluchowski's result, $M^E_\alpha = 1$, is recovered in the low-frequency limit, but

$$M^E_\alpha = B^\infty_\alpha / (\lambda [M^A_\alpha + (\rho_P/\rho)\, V_P])$$

in the high-frequency limit, indicating that $M^E_\alpha \sim \lambda^{-1}$ for $|\lambda| \gg 1$ regardless of the particle density. For moderate-aspect-ratio spheroids and cylinders, (3.6) may be inserted into (4.3) to yield simple algebraic expressions for the unsteady hydrodynamic and electrophoretic mobilities valid for all oscillation frequencies. In this article, we focus on $\boldsymbol{M}^E$ because of the link it provides between macroscopic electroacoustic measurements and suspension microstructure via O'Brien's (1990) reciprocal relation (1.2); the connection between $\boldsymbol{M}^0$ and acoustic dissipation is discussed in §6.

The unsteady electrophoretic mobilities of non-conducting randomly oriented spheroidal and cylindrical particles are depicted in figure 4, where $\langle M^E \rangle =$

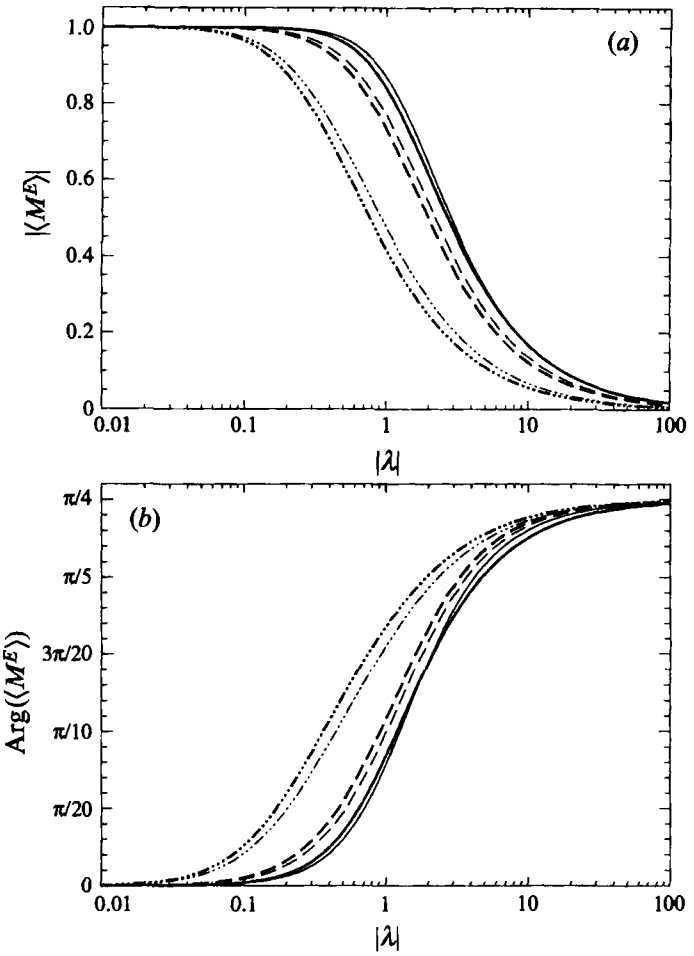

FIGURE 4. Magnitude (*a*) and phase angle (*b*) for the electrophoretic mobilities of randomly oriented non-conducting ($\epsilon_P/\epsilon = \tilde{K}^S = 0$) spheroids (thinner curves) and cylinders (thicker curves); the aspect ratios (ϕ = length/width) are: $\phi = 1$ (solid curves), $\phi = 10$ (dashed curves), and $\phi = 1/10$ (dashed-dotted curves). The density ratio is $\rho_P/\rho = 2$. The frequency parameter, λ, is based on the minimum overall particle dimension (half-width of rods and half-thickness of disks).

$\frac{1}{3}(M_{\parallel}^E + 2M_{\perp}^E)$. The results for a sphere are analytically described by O'Brien's (1988) formula; results for spheroids were obtained by Loewenberg & O'Brien (1992). The results for a finite-length cylinder are new. The limiting low- and high-frequency behaviours, discussed above, are apparent for $|\lambda| < 0.1$ and $|\lambda| > 10$. The results indicate that equal-aspect-ratio spheroids and finite-length cylinders behave almost identically; electroacoustic measurements will be insensitive to detailed geometrical features. It is also apparent that rod-shaped particles behave similarly to spheres. However, the results illustrated in figure 4 indicate that electroacoustic measurements may be able to distinguish disk-shaped particles. The effect of particle density is depicted in figure 5. Apparently, electrophoretic mobilities are sensitive to particle density; this parameter may therefore be accessible by electroacoustic measurements. The results shown in figure 5 indicate that the electrophoretic mobility of heavy particles decreases more rapidly with increasing frequency and can exhibit a phase angle maximum at $|\lambda| = O(1)$. Phase-angle overshoot occurs for globular particles

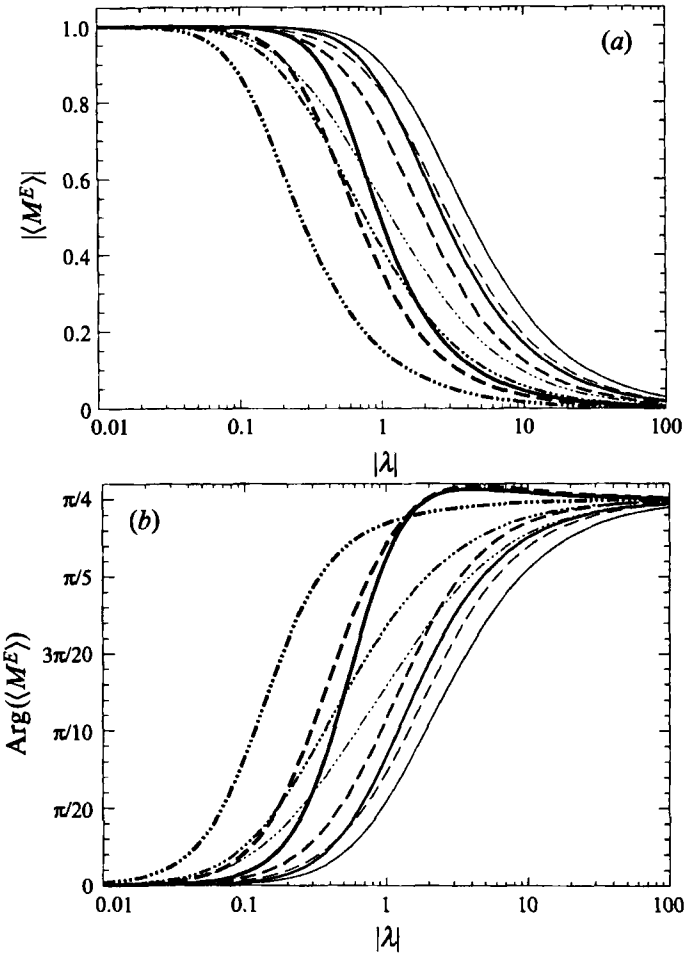

FIGURE 5. Magnitude (*a*) and phase angle (*b*) for the electrophoretic mobilities of randomly oriented non-conducting cylinders with density ratios: $\rho_P/\rho = 1$ (thinnest curves), $\rho_P/\rho = 2$ (medium thickness curves), $\rho_P/\rho = 10$ (thickest curves). $\phi = 1$ (solid curves), 10 (dashed curves), 1/10 (dashed-dotted curves). λ is defined as in figure 4.

($\phi \approx 1$) and rods with $\rho_P/\rho = 10$, but not for disks of the same density; for a sphere, it can be shown that phase-angle overshoot occurs if $\rho_P/\rho > 4$.

In the absence of an applied electric field, the particles are randomly oriented because of Brownian motion. However, in electroacoustic applications, the assumption that the particles are randomly oriented also requires that Brownian motion dominate the electrical alignment of the particles. Non-conducting particles have an induced dipole moment $\approx \epsilon a^3 V_P E^\infty$. Brownian motion will dominate electrical anisotropy if $\epsilon a^3 V_P E^{\infty 2}/kT \ll 1$. For a 1 μm particle in water at room temperature, in a typical electric field strength of 10 V cm^{-1}, $\epsilon a^3 V_P E^{\infty 2}/kT \sim 0.2$ and thus electrically induced anisotropy may be significant. The electric field will exert a torque of approximately $\epsilon a^3 V_p E^{\infty 2}$ on a non-conducting particle, resulting in rotation with angular velocity of approximately $\epsilon V_P E^{\infty 2}/\mu$; thus, electrical anisotropy will also be unimportant if $\epsilon \tau E^{\infty 2}/\mu \ll 1$, where τ is the length of time during which the electric field is applied across the suspension. In water, with a field strength of 10 V cm^{-1}, electrically induced anisotropy is established on the timescale $(\epsilon E^{\infty 2}/\mu)^{-1} \sim 1$ s, in contrast with $\tau \sim 10^{-4}$ s

for the existing pulsed-field electroacoustic devices. We conclude that in these instruments, the initially isotropic particle orientation distribution persists during the timescale of interest. Conducting particles have smaller induced dipole moments so random orientations are more likely. Thus, only results for orientationally isotropic suspensions are illustrated herein.

5. Conducting spheroidal particles

5.1. *Unsteady electrophoretic motion of conducting spheroids*

In a uniform applied electric field, $\boldsymbol{E}^{\infty}$, the intraparticle field in a homogeneous ellipsoid is uniform and given by (Stratton 1941; Landau, Lifshitz & Pitaevskii 1984)

$$\hat{\boldsymbol{E}} = \boldsymbol{L}\cdot\boldsymbol{E}^{\infty}; \quad L_{\alpha} = \frac{1+m_{\alpha}^{A}}{1+(K^{P}/K)\,m_{\alpha}^{A}}, \tag{5.1}$$

where K^{P} is the (volumetric) particle conductivity, $K = K^{\infty} - i\omega\epsilon$ is the fluid conductivity, and $\boldsymbol{m}^{A} = \boldsymbol{M}^{A}/V_{P}$ is the added-mass tensor normalized by the particle volume. Then, by (2.3), we can express the tangential field on the surface of a conducting ellipsoid as

$$\boldsymbol{E}_{t} = G_{\alpha}E^{\infty}\boldsymbol{E}_{0}; \quad G_{\alpha} = [1+(K^{P}/K)\,m_{\alpha}^{A}]^{-1}, \tag{5.2}$$

where $\boldsymbol{E}_{0}$ is the dimensionless (tangential) field on the surface of a non-conducting ellipsoid. From (2.5) and the linearity of the electro-osmotic problem, we obtain the following remarkably simple generalization of the non-conducting results obtained in §§3 and 4 for a conducting ellipsoid:

$$\boldsymbol{u}^{E}(\boldsymbol{x}) = G_{\alpha}\boldsymbol{u}_{0}^{E}(\boldsymbol{x}), \quad \boldsymbol{R}^{E} = \boldsymbol{G}\cdot\boldsymbol{R}_{0}^{E}, \quad \boldsymbol{M}^{E} = \boldsymbol{G}\cdot\boldsymbol{M}_{0}^{E}, \tag{5.3a–c}$$

where $\boldsymbol{u}_{0}^{E}(\boldsymbol{x})$, $\boldsymbol{R}_{0}^{E}$, and $\boldsymbol{M}_{0}^{E}$ denote results for a non-conducting ellipsoid, given by (3.4), (3.5) and (4.3b); the combined velocity field is obtained from (4.2) by multiplying the $E^{\infty}\epsilon\zeta/\mu$ term by G_{α}.

For moderately charged ($\tilde{K}^{S} = 0$) dielectric ellipsoids, $K^{P} = -i\omega\epsilon_{P}$, thus (5.2) becomes

$$G_{\alpha} = \frac{1+\lambda_{E}^{2}}{1+[(\epsilon_{P}/\epsilon)\,m_{\alpha}^{A}+1]\,\lambda_{E}^{2}}, \tag{5.4}$$

indicating that $G_{\alpha} = 1$ at low frequencies for all values of ϵ_{P}/ϵ and thus the Smoluchowski mobility is recovered; G_{α} exhibits dispersive behaviour for $|\lambda_{E}| = O(1)$, and $G_{\alpha} = [(\epsilon_{P}/\epsilon)\,m_{\alpha}^{A}+1]^{-1}$ for $|\lambda_{E}| \gg 1$. Thus, high-frequency mobilities are reduced, but low-frequency mobilities are unaffected by large particle dielectric constants. From (5.3c), (5.4), and the values for $m_{\parallel}^{A}$ and $m_{\perp}^{A}$ listed in table 1, we conclude that the axial electrophoretic mobility of disk-shaped particles should be very sensitive to the particle dielectric constant. For $\phi \ll 1$, $m_{\parallel}^{A} = 2/\pi\phi$ (Loewenberg 1993b); thus, $M_{\parallel}^{E}$ is significantly reduced for $\epsilon_{P}/\epsilon \geqslant O(\phi)$. For $\phi \geqslant 1$, the transverse electrophoretic mobility is moderately sensitive to ϵ_{P}/ϵ ($m_{\perp}^{A} = 1$ for $\phi \gg 1$). The transverse mobility of oblate spheroids and the axial mobility of prolate spheroids are insensitive to the particle dielectric constant.

Formula (5.4) was obtained by Loewenberg & O'Brien (1992) but results were illustrated only for $\epsilon_{P}/\epsilon = 0$. The electrophoretic mobilities of moderately charged ($\tilde{K}^{S} = 0$) randomly oriented spheroids with large dielectric constants are depicted in figure 6. The results confirm that disk-shaped particles are most sensitive to the particle

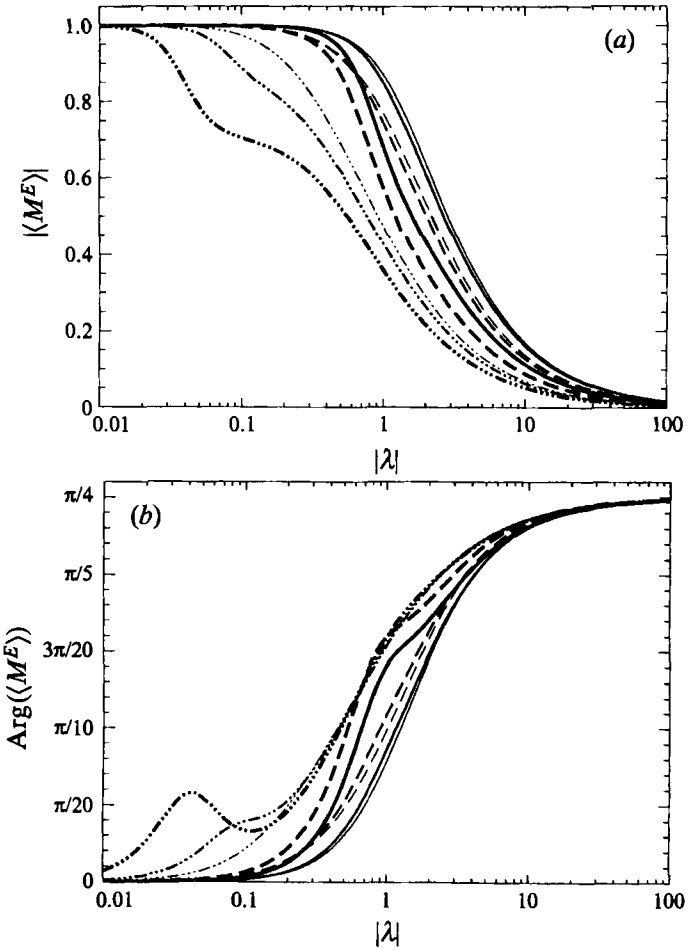

FIGURE 6. Magnitude (*a*) and phase angle (*b*) for the electrophoretic mobilities of randomly oriented moderately charged ($\tilde{K}^S = 0$) spheroids; $\epsilon_p/\epsilon = 0$ (thinnest curves), $\epsilon_p/\epsilon = 1/10$ (medium thickness curves), and $\epsilon_p/\epsilon = 1$ (thickest curves). $\phi = 1$ (solid curves), 10 (dashed curves), 1/10 (dashed-dotted curves). λ is defined as in figure 4; $a(\tilde{K}^\infty/\epsilon\nu)^{1/2} = 1$, thus $\lambda_E = \lambda$ and $\rho_p/\rho = 2$.

	$\phi = 1/10$	$\phi = 1/5$	$\phi = 1/2$	$\phi = 1$	$\phi = 2$	$\phi = 5$	$\phi = 10$
$m_{\parallel}^A$	6.18	3.01	1.12	0.500	0.210	0.0592	0.0207
$D_{\parallel} m_{\parallel}^A$	46.6	16.9	3.72	1.00	0.464	0.137	0.0484
$m_{\parallel}^A$	0.0747	0.142	0.310	0.500	0.704	0.893	0.962
$D_{\perp} m_{\perp}^A$	0.113	0.217	0.515	1.00	1.03	1.11	1.15

TABLE 1. Numerical values for the dimensionless hydrodynamic parameters that determine the conductivity factor, $\boldsymbol{G}$, and dipole moment, $\boldsymbol{S}$, of spheroidal particles according to (5.3), (5.9), and (5.12). $\boldsymbol{m}^A$ is the added mass, normalized by the particle volume; $\boldsymbol{D}$ is defined by (5.7), and is normalized by the minimum overall particle dimension (cross-sectional radius of prolate particles and half-thickness of oblate particles). ϕ is the aspect ratio

dielectric constant; electroacoustic measurements may be able to determine the dielectric constant of disk-shaped particles. According to (5.4) and the values in table 1, a sphere should be most sensitive to very large values of ϵ_P/ϵ because the mobility of non-spherical particles in the direction of least hydrodynamic resistance is insensitive to the particle dielectric constant; however, this prediction is not manifest in figure 6 for the largest particle dielectric constant considered ($\epsilon_P/\epsilon = 1$) and, therefore, it may not occur in practice.

For $\tilde{K}^S \neq 0$, an equivalent volumetric particle conductivity tensor is defined by equating the low-frequency ($|\lambda_E| \ll 1$) electrical dissipation rate for an ellipsoid with only surface conduction to that of an ellipsoid with only volumetric conduction. We shall assume that the electric field for an ellipsoid with surface conductivity, K^S, is approximately the same as that for an ellipsoid with a volumetric conductivity, K^P; thus, electrical dissipation outside the two particles is the same. Electrical dissipation resulting from surface conduction is equated to that caused by conduction within an ellipsoid volume. Accordingly, we write

$$K^S \int_{S_P} \boldsymbol{E}\cdot\boldsymbol{E}\,\mathrm{d}S = aK_\alpha^P \int_{V_p} \hat{\boldsymbol{E}}\cdot\hat{\boldsymbol{E}}\,\mathrm{d}V. \tag{5.5}$$

By (5.1), (5.5) can be rewritten as

$$K^S \int_{S_P} \boldsymbol{E}_0\cdot\boldsymbol{E}_0\,\mathrm{d}S = aK_\alpha^P(1+m_\alpha^A)^2 V_P. \tag{5.6}$$

By inserting (3.2) into the expression for $\boldsymbol{B}^\infty$ given beneath (3.7), we find

$$\int_{S_P} (\boldsymbol{E}_0\cdot\boldsymbol{E}_0)\,\mathrm{d}S = B_\alpha^\infty;$$

thus,
$$\boldsymbol{K}^P = \frac{K^S}{a}\boldsymbol{D}, \quad D_\alpha = \frac{B_\alpha^\infty/V_P}{(1+m_\alpha^A)^2}. \tag{5.7}$$

If $\epsilon_P/\epsilon \neq 0$, then $\boldsymbol{K}^P = (K^S/a)\boldsymbol{D} - i\omega\epsilon_P\boldsymbol{I}$, where $\boldsymbol{I}$ is the isotropic second-order tensor.

The above result depends critically on the assumption preceding (5.5) regarding the electric field for an ellipsoid with surface conductivity. Fortunately, Dukhin & Shilov (1980) performed exact numerical calculations for the low-frequency electrical conductivity of a dilute suspension of highly charged spheroids ($\tilde{K}^S \neq 0$) and their results support this conjecture. For moderate-aspect-ratio spheroids ($1/10 \leqslant \phi \leqslant 10$), Dukhin & Shilov observed that their exact calculations were accurately approximated ($\approx 5\%$) by a simple analytical form, derived by satisfying (2.2) in an integral sense only. The validity of this approximation was confirmed by O'Brien & Ward (1988) who applied Dukhin & Shilov's numerical method to calculate the quasi-steady electrophoretic mobility of a highly charged spheroid. O'Brien & Rowlands (1993) empirically confirmed the Dukhin–Shilov approximation in the context of determining the high-frequency electrical conductivity of a dilute suspension of highly charged oblate spheroids; this finding is particularly important because it supports application of the Dukhin–Shilov approximation to the high-frequency conditions of interest herein. Dukhin & Shilov (1980) showed that an equivalent volumetric particle conductivity tensor, $\boldsymbol{K}^P$, can be rigorously identified with their approximation; formulae for the principal values K_α^P were given, which are equivalent to (5.7). The intuitive derivation of this result, contained herein, provides a physical basis for the mathematical equivalence, and it suggests the possibility of generalizing the Dukhin–Shilov approximation to ellipsoids.

Substituting (5.7) into (5.2) yields

$$G_\alpha = \frac{1+\lambda_E^2}{1+\tilde{K}^S D_\alpha m_\alpha^A + \lambda_E^2} \tag{5.8}$$

for highly charged spheroids with small dielectric constants ($\epsilon_P/\epsilon = 0$, $\tilde{K}^S \neq 0$). In this case, $G_\alpha = [1+K_\alpha^S D_\alpha m_\alpha^A]^{-1}$ for $|\lambda_E| \ll 1$, and $G_\alpha \to 1$ at high frequencies; G_α exhibits dispersion for $|\lambda_E| = O(1)$. Surface conductivity reduces low- but not high-frequency particle mobilities. The Smoluchowski result, $M^E = 1$, is not recovered for $|\lambda| \to 0$ because it does not describe the quasi-steady electrophoretic migration of highly charged particles (Dukhin & Derjaguin 1974; O'Brien 1983; O'Brien & Ward 1988). Equations (5.3*c*) and (5.8) generalize O'Brien's (1988) formula to highly charged spheroidal particles. The values for $D_\parallel m_\parallel^A$ and $D_\perp m_\perp^A$ listed in table 1 indicate that the axial, but not the transverse, electrophoretic mobility of disk-shaped particles should be extremely sensitive to the surface conductivity of the particle. The converse is true for $\phi \geqslant 1$: only the transverse electrophoretic mobility is modestly sensitive to $\tilde{K}^S$ ($D_\parallel m_\parallel^A \approx 1$). The transverse mobility of oblate spheroids and the axial mobility of prolate spheroids depend weakly on $\tilde{K}^S$.

In figure 7, the electrophoretic mobilities of highly charged randomly oriented spheroids with small dielectric constants ($\epsilon_P/\epsilon = 0$) are depicted. The results confirm that disk-shaped particles are extremely sensitive to surface conductivity. From (5.8) and the values in table 1, we deduce that $M_\parallel^E$ for an oblate spheroid ($\phi = 1/10$) is reduced by 32% at low frequencies by a very slight surface conductivity, $\hat{K}^S = 1/100$, whilst $M_\perp^E$ is essentially unaffected; the resulting approximately 11% reduction in the quasi-steady electrophoretic mobility of randomly oriented oblate spheroids is evident in figure 7. Low-frequency electroacoustic measurements may be able to yield the surface conductivity of disk-shaped particles, providing access to further microstructural details of the suspension. Figure 7 indicates that spherical and prolate particles are an order of magnitude less sensitive to small but non-zero surface conductivity. However, the results indicate that a spherical particle is most sensitive to large surface conductivities because the electrophoretic mobilities of non-spherical particles in the direction of least hydrodynamic resistance are only weakly affected by surface conductivity, as the values in table 1 indicate.

For the general case $\epsilon_P/\epsilon \neq 0$, $\tilde{K}^S \neq 0$, the electro-osmotic fluid velocity, resistance, and electrophoretic mobility of conducting spheroids are modified (relative to the quantities for non-conducting particles) according to (5.3), where

$$G_\alpha = \frac{1+\lambda_E^2}{1+\tilde{K}^S D_\alpha m_\alpha^A + (\epsilon_P/\epsilon+1)\lambda_E^2} \tag{5.9}$$

with requisite parameter values given in table 1. Contrasting figures 4 and 5 with figures 6 and 7, reveals a complex dispersive behaviour in an intermediate frequency range that is attributable to particle conductivity. This behaviour is very weakly modulated by the value of $a(K^\infty/\epsilon\nu)^{1/2}$. The results depicted in figures 6 and 7 correspond to $a(K^\infty/\epsilon\nu)^{1/2} = 1$ ($\lambda_E = \lambda$); qualitatively similar results were observed for $a(K^\infty/\epsilon\nu)^{1/2} = 0.1$ and 10.

5.2. *High-frequency electrical conductivity*

According to the reciprocal relation (1.2) electroacoustic measurements require high-frequency electrophoretic mobilities and suspension conductivities. For dilute suspensions of spheroids, the conductivity is given by the formula (5.12), which is

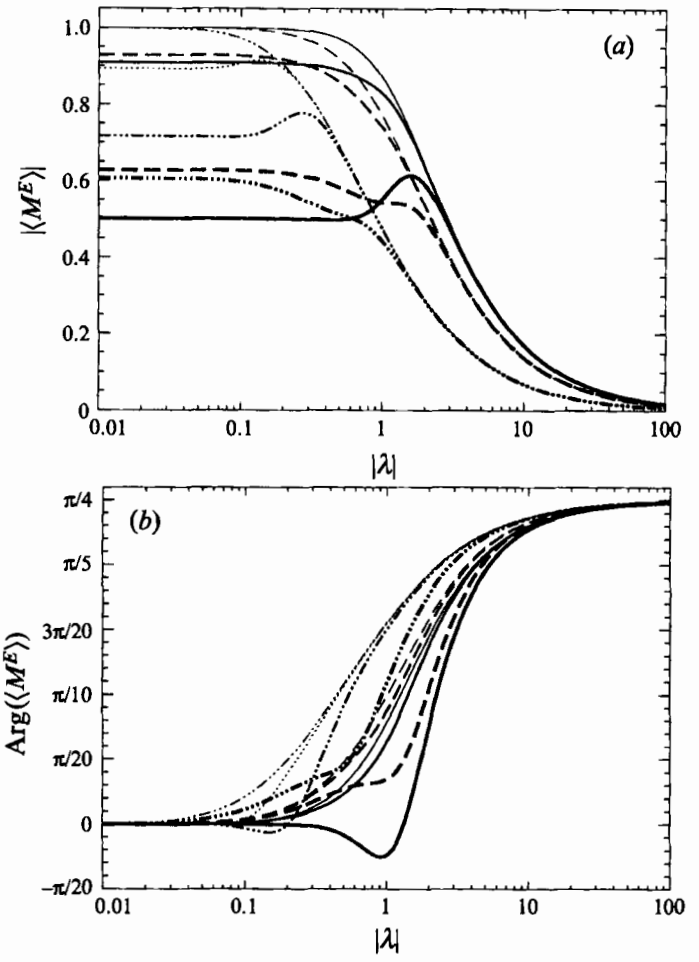

FIGURE 7. Magnitude (*a*) and phase angle (*b*) for the electrophoretic mobilities of randomly oriented highly charged spheroids with small dielectric constants ($\epsilon_P/\epsilon = 0$); $\tilde{K}^S = 0$ (thinnest curves), $\tilde{K}^S = 1/10$ (medium thickness curves), and $\tilde{K}^S = 1$ (thickest curves). $\phi = 1$ (solid curves), 10 (dashed curves), 1/10 (dashed-dotted curves); an additional dotted curve depicts the mobility for $\tilde{K}^S = 1/100$, $\phi = 1/10$. λ is defined as in figure 4; $a(K^\infty/\epsilon\nu)^{1/2} = 1$, thus $\lambda_E = \lambda$ and $\rho_P/\rho = 2$.

derived below by generalizing the low-frequency ($10^3 \ll \omega \ll 10^6$ rad s^{-1}) results of Dukhin & Shilov (1980) and the results of Fricke (1953) for dielectric particles.

The suspension conductivity that appears in (1.2) is defined by (Russel *et al.* 1989)

$$\frac{\boldsymbol{K}^*}{K} = \boldsymbol{I} + c\boldsymbol{S}; \quad \boldsymbol{S} = \frac{1}{V_P}\left(\frac{\boldsymbol{K}^P}{K} - \boldsymbol{I}\right) \cdot \int_{V_P} \hat{\boldsymbol{E}}\, \mathrm{d}V, \tag{5.10}$$

where $\boldsymbol{S}$ is the electric dipole moment of the particle. Displacement currents are negligible under low-frequency conditions, thus the particle conductivity is described by (5.7) and the fluid conductivity is given by $K = K^\infty$. Then, with the help of (5.1), the dipole moment is evaluated and the result of Dukhin & Shilov (1980) is recovered:

$$S_\alpha = \frac{(\tilde{K}^S D_\alpha - 1)(1 + m_\alpha^A)}{1 + \tilde{K}^S D_\alpha m_\alpha^A}. \tag{5.11}$$

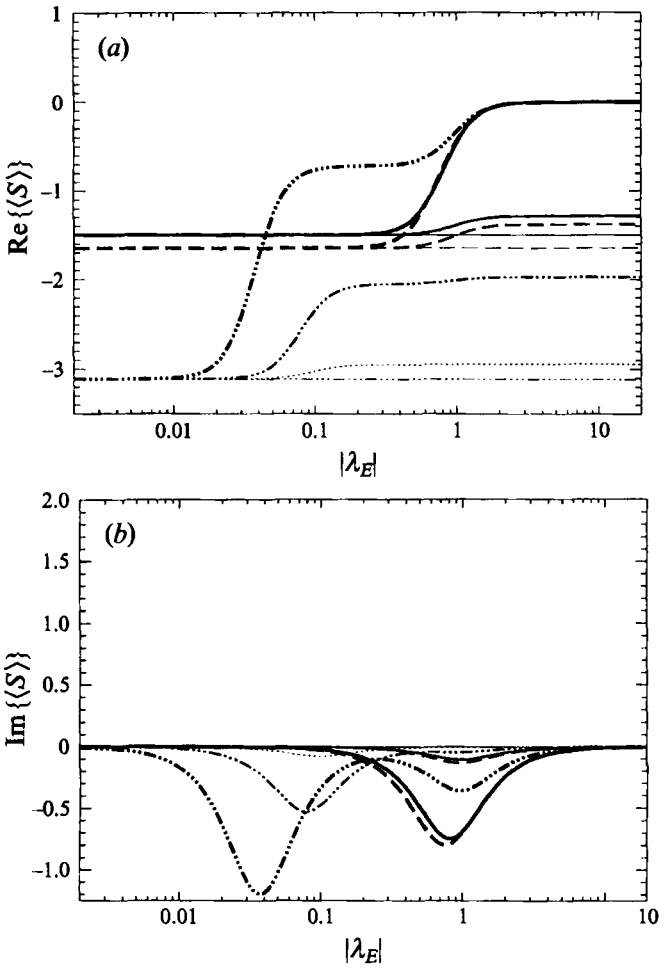

FIGURE 8. Real (*a*) and imaginary (*b*) parts of the dipole moment for randomly oriented moderately charged ($\tilde{K}^S = 0$) spheroids; $\epsilon_P/\epsilon = 0$ (thinnest curves), $\epsilon_P/\epsilon = 1/10$ (medium thickness curves), and $\epsilon_P/\epsilon = 1$ (thickest curves). $\phi = 1$ (solid curves), 10 (dashed curves), 1/10 (dashed-dotted curves); an additional, dotted curve depicts the dipole moment for $\epsilon_P/\epsilon = 1/100$, $\phi = 1/10$.

The result is easily generalized to high frequency by including displacement currents in the particle and suspending fluid; thus, $\boldsymbol{K}^P = (K^S/a)\boldsymbol{D} - \mathrm{i}\omega\epsilon_P \boldsymbol{I}$, and $K = K^\infty - \mathrm{i}\omega\epsilon$. The result is

$$S_\alpha = \frac{[(\tilde{K}^S D_\alpha - 1) + (\epsilon_P/\epsilon - 1)\lambda_E^2](1 + m_\alpha^A)}{1 + \tilde{K}^S D_\alpha m_\alpha^A + (1 + m_\alpha^A \epsilon_P/\epsilon)\lambda_E^2}, \tag{5.12}$$

which is valid for $10^3 \ll \omega \ll 10^9$ rad s^{-1}; (5.11) is recovered in the low-frequency limit, and $S_\alpha = (\epsilon_P/\epsilon - 1)(1 + m_\alpha^A)(1 + m_\alpha^A \epsilon_P/\epsilon)^{-1}$ for $|\lambda_E| \gg 1$. For $\tilde{K}^S = 0$, the result reduces to the well-established Maxwell–Wagner theory for spheroids (Russel *et al.* 1989; Fricke 1953):

$$S_\alpha = \frac{[(\epsilon_P/\epsilon - 1)\lambda_E^2 - 1](1 + m_\alpha^A)}{1 + (1 + m_\alpha^A \epsilon_P/\epsilon)\lambda_E^2}, \tag{5.13}$$

which has the same high-frequency limit as (5.12). Thus, (5.11) and (5.13) are special cases of (5.12). Recently, the observation that these regimes are linked according to

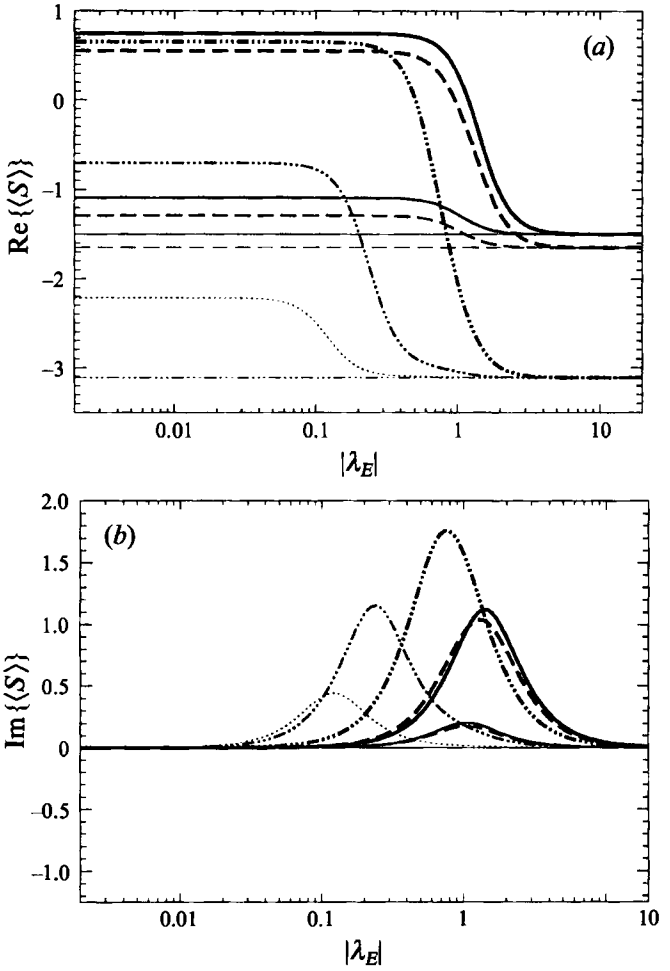

FIGURE 9. Real (*a*) and imaginary (*b*) parts of the dipole moment for randomly oriented highly charged spheroids with small dielectric constants ($\epsilon_P/\epsilon = 0$); $\tilde{K}^S = 0$ (thinnest curves), $\tilde{K}^S = 1/10$ (medium thickness curves), and $\tilde{K}^S = 1$ (thickest curves). $\phi = 1$ (solid curves), 10 (dashed curves), and 1/10 (dashed-dotted curves); an additional, dotted curve depicts the dipole moment for $\tilde{K}^S = 1/100$, $\phi = 1/10$.

(5.12) was independently made by O'Brien & Rowlands (1993) who experimentally confirmed the result for disk-shaped particles. Equations (5.10) and (5.12) generalize the O'Brien–Rowlands formula to include rod-shaped particles and they establish a useful connection between well-known inviscid flow parameters and the electrical conductivity of a dilute suspension of spheroids with arbitrary charge and dielectric constant; the required parameter values are supplied in table 1.

Similarly to the results for electrophoretic particle mobilities, (5.12) and the parameter values listed in table 1 indicate that the dipole moment of an oblate spheroid aligned with the applied field is very sensitive to dielectric constant and surface conductivity; $S_\perp$ for an oblate spheroid and $S_\parallel$ for a prolate spheroid are insensitive to ϵ_P/ϵ or $\tilde{K}^S$. The dipole strength of moderately charged ($\tilde{K}^S = 0$), spheroids are depicted in figure 8; highly charged spheroids with small dielectric constants ($\epsilon_P/\epsilon = 0$) are shown in figure 9. The depicted results thus correspond, respectively, to the Maxwell–Wagner theory (5.13), and the low-frequency Dukhin–Shilov result (5.11).

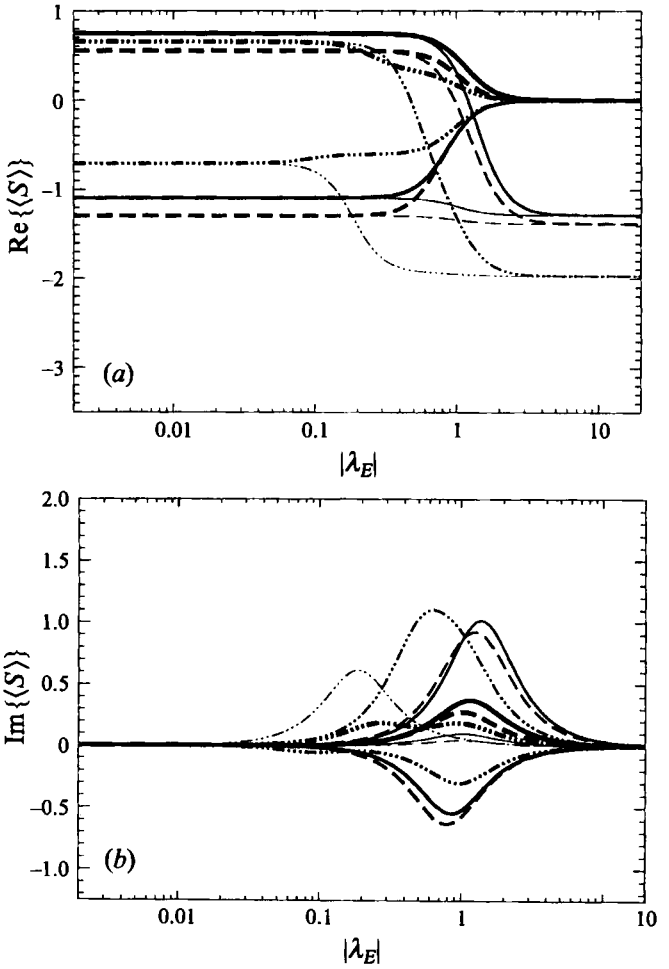

FIGURE 10. Real (*a*) and imaginary (*b*) parts of the dipole moment for randomly oriented highly charged spheroids with large dielectric constants; $\epsilon_P/\epsilon = \tilde{K}^S = 1/10$ (thinnest curves), $\epsilon_P/\epsilon = 1/10$, $\tilde{K}^S = 1$ (second thinnest curves), $\epsilon_P/\epsilon = 1$, $\tilde{K}^S = 1/10$ (second thickest curves), and $\epsilon_P/\epsilon = \tilde{K}^S = 1$ (thickest curves). $\phi = 1$ (solid curves), 10 (dashed curves), 1/10 (dashed-dotted curves).

The dipole strength of highly charged spheroids with large dielectric constants is illustrated in figure 10. Dispersive behaviour is evident in all figures for $|\lambda_E| = O(1)$; the results depicted in figure 10 indicate that the dispersive effects of particle dielectric constant and surface conductivity tend to cancel each other. By the arguments given at the end of §4, orientational isotropy is assumed: $\langle S \rangle = \frac{1}{3}(S_\parallel + 2S_\perp)$.

As predicted, the results depicted in figures 8–10 reveal that disk-shaped particles are most sensitive to particle conductivity. For $\epsilon_P/\epsilon = 1/100$, figure 8 shows that the dipole moment of an oblate spheroid is affected comparably to that of a sphere or prolate spheroid with an order to magnitude larger particle dielectric constant; for $\tilde{K}^S = 1/100$, figure 9 indicates that the dipole moment of an oblate spheroid is *more* affected than that of a sphere or prolate spheroid with a ten-fold greater surface conductivity. Figure 8 reveals two distinct characteristic relaxation frequencies for disk-shaped dielectric particles; the behaviour is most apparent for $\epsilon_P/\epsilon = 1$ but it can also be discerned for $\epsilon_P/\epsilon = 1/10$. From the parameter values in table 1, we deduce that the lower relaxation

frequency corresponds to $S_{\parallel}$, and the higher frequency relaxation to $S_{\perp}$. The results depicted in figure 10 indicate that the double-dispersive behaviour of moderately charged disk-shaped particles with large dielectric constants is largely suppressed for $\hat{K}^S = 1/10$. The results shown in figures 8–10 indicate that rod-shaped particles behave remarkably like spheres. In addition to their electroacoustic application, high-frequency conductivity measurements may be able to independently determine the aspect ratio, dielectric constant, and surface conductivity of disk-shaped particles; particle shape cannot be inferred from conductivity measurements if $\phi \geqslant 1$.

6. Electroacoustic energy dissipation in a dilute suspension

The performance of electroacoustic devices is degraded by energy dissipation. In this section, we analyse the energy dissipation in a dilute suspension subjected simultaneously to sound waves and electric fields, the situation that arises during electroacoustic measurements.

For a dilute suspension, the macroscopic electroacoustic equations are (O'Brien 1990)

$$-\mathrm{i}\omega\rho\left[\boldsymbol{U}^{\infty}+c\frac{\Delta\rho_P}{\rho}\boldsymbol{U}^{P}\right]=-\boldsymbol{\nabla}P^{\infty},\quad \rho\boldsymbol{\nabla}\cdot\boldsymbol{U}^{\infty}=\mathrm{i}\omega\chi P^{\infty},\quad \boldsymbol{\nabla}\cdot\boldsymbol{J}^{\infty}=0,\quad (6.1\,a\text{–}c)$$

where an $\mathrm{e}^{-\mathrm{i}\omega t}$ time dependence has been assumed, which is valid because of the linearity of the electroacoustic equations and consistent with the development herein. The particle velocity and current density are described by (1.1) and (1.2). The term $\rho[\boldsymbol{U}^{\infty}+c(\Delta\rho_P/\rho)\,\boldsymbol{U}^{P}]$ in the force balance (6.1 *a*) is the momentum per unit volume of suspension; only pressure forces are retained in the force balance because they dominate the viscous and interparticle forces if the wavelength of sound is large compared to the particle size at the frequency ω (O'Brien 1990). In the neighbourhood of a given particle, the suspension is locally incompressible, as explained in §2.2; macroscopically, however, the suspension is compressible as (6.1 *b*) indicates, and χ is the bulk compressibility. Conservation of charge results in (6.1 *c*). Together these five equations (1.1), (1.2) and (6.1) determine the average particle velocity, current density, macroscopic fluid velocity and pressure, and macroscopic electric field subject to the appropriate macroscopic boundary conditions that arise from conservation of mass, momentum, and charge density.

The macroscopic energy flux in a suspension is $\boldsymbol{e} = P^{\infty}\boldsymbol{U}^{\infty} + \Psi^{\infty}\boldsymbol{J}^{\infty}$, where Ψ^{∞} is the electric potential, $\boldsymbol{E}^{\infty} = -\boldsymbol{\nabla}\Psi^{\infty}$. The (time-averaged) volumetric electroacoustic dissipation rate is

$$\dot{e} = \overline{\mathrm{Re}\{\boldsymbol{\nabla}\cdot\boldsymbol{e}\}} = \tfrac{1}{2}\mathrm{Re}\{\boldsymbol{\nabla}\tilde{P}^{\infty}\cdot\boldsymbol{U}^{\infty} + \tilde{P}^{\infty}\boldsymbol{\nabla}\cdot\boldsymbol{U}^{\infty} - \tilde{\boldsymbol{E}}\cdot\boldsymbol{J}^{\infty} + \tilde{\Psi}\boldsymbol{\nabla}\cdot\boldsymbol{J}^{\infty}\},\qquad (6.2)$$

where the overbar denotes a time average over the oscillation period, $2\pi/\omega$, and the tilde denotes a complex-conjugate quantity; $\overline{\mathrm{Im}\{\boldsymbol{\nabla}\cdot\boldsymbol{e}\}}$ is the average stored energy. With the help of (1.1), (1.2), (4.3 *a*), (5.10), (5.12), and (6.1), we obtain

$$-\dot{e} = \frac{1}{2}\frac{\omega}{\rho}\mathrm{Im}\{\chi\}|P^{\infty}|^2 + \tfrac{1}{2}K^{\infty}|E^{\infty}|^2 + c\left[\frac{\beta}{\rho\omega}|\boldsymbol{\nabla}P^{\infty}|^2 + K^{\infty}\gamma|E^{\infty}|^2\right] + O(c^2),\qquad (6.3)$$

where β and γ are the dimensionless viscous and electrical dissipation coefficients for the suspended particles, given by (6.4) below. An interesting feature of the result is the independence of electrical and viscous contributions despite their interaction via (1.2); they can be independently derived by considering a suspension subjected solely to electric fields or sound waves.

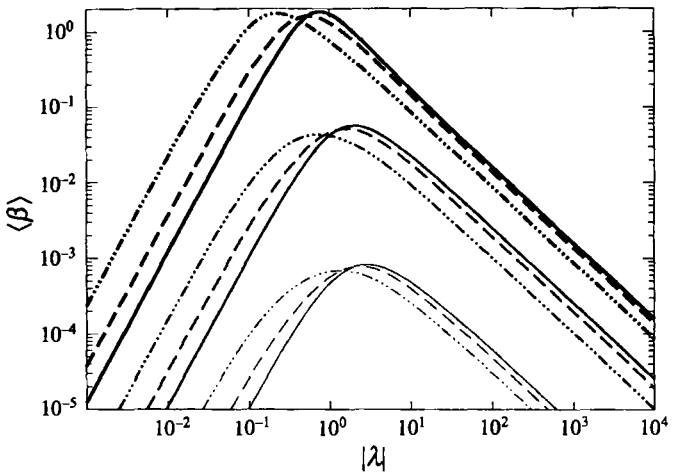

FIGURE 11. Viscous dissipation coefficient for randomly oriented spheroids with density ratios: $\rho_P/\rho = 1.1$ (thinnest curves), $\rho_P/\rho = 2$ (medium thickness curves), $\rho_P/\rho = 10$ (thickest curves). $\phi = 1$ (solid curves), 10 (dashed curves), 1/10 (dashed-dotted curves). λ is defined as in figure 4.

The $O(c)$ term in (6.3) results exclusively from the suspended particles. The viscous and electrical dissipation coefficients are given by

$$\beta_\alpha = \frac{1}{2}\frac{\Delta\rho}{\rho}\operatorname{Im}\{M_\alpha^0\} = \frac{1}{2}\frac{\operatorname{Re}\{R_\alpha^0\}|\lambda|^2(\Delta\rho_P/\rho)^2 V_P}{|R_\alpha^0+\lambda^2(\rho_P/\rho)V_P|^2}; \tag{6.4a}$$

$$\gamma_\alpha = \tfrac{1}{2}[\operatorname{Re}\{S_\alpha\}+|\lambda_E|^2\operatorname{Im}\{S_\alpha\}]$$
$$= \frac{1}{2}\frac{(\tilde{K}^S D_\alpha - 1)(\tilde{K}^S D_\alpha m_\alpha^A + 1) + [(\epsilon_P/\epsilon)^2 m_\alpha^A - 2(\epsilon_P/\epsilon)m_\alpha^A + \tilde{K}^S D_\alpha(m_\alpha^A+1) - 1]|\lambda_E|^4}{(1+\tilde{K}^S D_\alpha m_\alpha^A)^2 + [1+(\epsilon_P/\epsilon)m_\alpha^A]|\lambda_E|^4}$$
$$\times(1+m_\alpha^A), \tag{6.4b}$$

where $\langle\beta\rangle = \frac{1}{3}(\beta_\parallel + 2\beta_\perp)$, and $\langle\gamma\rangle = \frac{1}{3}(\gamma_\parallel + 2\gamma_\perp)$ for orientationally isotropic suspensions as assumed herein by the arguments given at the end of §4.

The non-negative term involving $\operatorname{Im}\{\chi\}$ in (6.3) arises from the expansion viscosity of the fluid (Lighthill 1978) and also from thermal dissipation associated with the differential adiabatic heating and cooling of the particles relative to the surrounding fluid as a result of pressure fluctuations; generally, thermal dissipation occurs if the oscillation period is comparable to the thermal relaxation time of the particle (Temkin 1981). Other sources for $\operatorname{Im}\{\chi\} > 0$ are discussed by O'Brien (1990). The $O(c)$ term in (6.3) involving β describes viscous dissipation associated with relative fluid-particle motion. Viscous dissipation usually dominates thermal dissipation except for particles of near neutral buoyancy (Allegra & Hawley 1971); furthermore, viscous dissipation often dominates the entire $\operatorname{Im}\{\chi\}$ term except at exceedingly high frequencies, or if the suspension is extremely dilute or contains microscopic bubbles (Lighthill 1978). Viscous dissipation results in exponential acoustic energy loss, $4\pi c\langle\beta\rangle$ per wavelength, and causes the amplitude of a plane sound wave to decay exponentially at half this rate. According to (6.4*a*), the viscous dissipation coefficient is non-negative and vanishes only if $\Delta\rho_P = 0$. Except for $\rho_P/\rho \ll 1$, $\langle\beta\rangle$ attains a maximal value, $O(\Delta\rho_P^2/\rho\rho_P)$ at $|\lambda| \sim (\rho/\rho_P)^{1/2}$ (Loewenberg 1994*b*). The results depicted in figure 11 illustrate these features and reveal that disc-shaped particles are somewhat distinct but rods behave as spheres; more extensive results are given by Loewenberg (1994*b*).

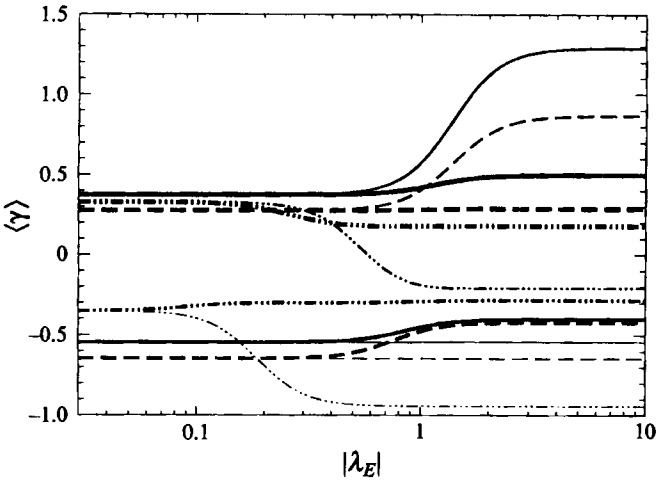

FIGURE 12. Electrical dissipation coefficient for randomly oriented highly charged spheroids with large dielectric constants; $\epsilon_p/\epsilon = \tilde{K}^s = 1/10$ (thinnest curves), $\epsilon_p/\epsilon = 1/10$, $\tilde{K}^s = 1$ (second thinnest curves), $\epsilon_p/\epsilon = 1$, $\tilde{K}^s = 1/10$ (second thickest curves), and $\epsilon_p/\epsilon = \tilde{K}^s = 1$ (thickest curves). $\phi = 1$ (solid curves), 10 (dashed curves), 1/10 (dashed-dotted curves).

The $\frac{1}{2}K^\infty|E^\infty|^2$ term in (6.3) results from resistive electrical heating of the fluid; the subdominant contribution involving γ arises from the $O(c)$ modification of the suspension conductivity associated with the particles. The fraction of electrical energy converted to heat during each oscillation period is $4\pi|\lambda_E|^{-2}$ $(\frac{1}{2}+c\langle\gamma\rangle)$. According to (6.4*b*) and the results shown in figure 12, γ depends monotonically on frequency, has finite low- and high-frequency limits, and has an undetermined sign. Figures 11 and 12 indicate that the electrical and viscous dissipation coefficients exhibit a similar sensitivity to particle shape. As expected, $\dot{\epsilon} < 0$ always.

It is interesting to consider the electrical dissipation induced by sound waves in a suspension, and conversely, the viscous dissipation caused by electrophoretic particle motion. In the first case, we obtain an estimate of the electric field from (1.2) with $\boldsymbol{J}^\infty = 0$; in the second case, we estimate the pressure gradient from (6.1*a*) with $\boldsymbol{U}^\infty = 0$. In either case, with the help of (4.3) and (6.4), we find that the ratio of the induced energy dissipation to the primary dissipation, associated with the applied field, is approximately $10^{-3}c(\zeta/\kappa a)^2$ under quite general conditions relevant to electroacoustic measurements in aqueous suspensions, where the $\zeta-$potential is in mV. Recalling that $\kappa a \gg 1$ and $\zeta \leqslant O(100\text{ mV})$, we conclude that the interaction of electrical and acoustic energy is negligible, even in concentrated suspensions. Together, this result and (6.3) indicate that electroacoustic energy dissipation can be accurately estimated by considering each applied field acting independently.

7. Concluding remarks

The unsteady electrophoretic motion of a non-spherical colloidal particle has been investigated. A microphysical understanding of the electroacoustic measurement process will be advanced by the new qualitative features of the electro-osmotic flow field and particle resistance that are presented in this article. Under practical relevant conditions, it is assumed and justified that the fluid is locally incompressible, the Reynolds number (based on particle size) is small, and the electric double layer is thin

compared to the particle size. New results were obtained for the electrophoretic mobilities of highly charged and cylindrical particles, the high-frequency conductivity of highly charged spheroids, and the rate of electroacoustic energy dissipation in a dilute suspension. Each of these quantities should directly further practical applications of electroacoustic measurements.

It was shown that the electro-osmotic flow field past a stationary non-conducting electrically charged particle is a superposition of unsteady Stokes flow and potential flow past an oscillating particle with no applied field. The results indicate that the unsteady electro-osmotic flow field is insensitive to particle geometry. The unsteady electro-osmotic resistance tensor for a non-conducting particle equals its unsteady Stokes resistance minus its added mass. For moderate-aspect-ratio spheroids and cylinders, a simple formula accurately approximates the electro-osmotic resistance at all oscillation frequencies in terms of the steady Stokes resistance and Basset force tensors.

An expression for the unsteady electrophoretic mobility of non-conducting particles was obtained by a force balance. The result depends explicitly on particle density, and depends implicitly on particle shape through the dimensionless unsteady Stokes resistance, added mass, and volume; particle size enters explicitly through the viscous frequency parameter. For a fixed oscillation frequency, the results reveal a strong dependence on size, a moderate dependence on particle density, and a weaker shape dependence. Rod-shaped particles behave much like spheres but disk-shaped particles are distinct; the unsteady electrophoretic motion of equal-aspect-ratio spheroidal and cylindrical particles is very similar. According to a reciprocal relation, electroacoustic measurements are proportional to the volume fraction, ζ-potential, and electrophoretic mobility of the suspended particles. We conclude that while quasi-steady electrophoresis and electroacoustic measurements can both determine the ζ-potential of a particle, electroacoustic measurements may also be able to determine particle size, density, and volume fraction, and possibly distinguish disk-shaped particles, but not rods, from spheres; however, electroacoustic measurements are insensitive to detailed geometric features of the particle surface.

Exploiting a special property of ellipsoids, the results for non-conducting particles were generalized to incorporate the effect of displacement currents or double-layer conduction in dielectric or highly charged moderate-aspect-ratio spheroids. The results for conducting particles are related to the results for non-conducting particles by a complex-valued multiplicative factor that depends explicitly on the particle dielectric constant and surface conductivity; only the added-mass and Basset-force tensors are needed, and the requisite parameters are supplied. Since these parameters are needed for non-conducting particles, results for conducting spheroids are obtained without further calculation. Results indicate that the unsteady electrophoretic motion of oblate spheroids is very sensitive to its dielectric constant and surface conductivity; the mobilities of prolate spheroids and spheres are much less sensitive to particle conductivity, and their behaviour is similar. We conclude that electroacoustic measurements may yield additional microstructural information in suspensions of disk-shaped particles that are highly charged or have large dielectric constants.

A formula was obtained for the high-frequency electrical conductivity of a dilute suspension of spheroids with arbitrary charge and dielectric constant; only the added-mass and Basset-force tensors are needed and the principal values are supplied. The formula depends explicitly on the particle dielectric constant, surface conductivity, and volume fraction; particle shape enters implicitly. According to the reciprocal relation, the high-frequency conductivity and electrophoretic mobility are both required for

electroacoustic measurements. High-frequency conductivity measurements may be independently useful for determining particle volume fraction, dielectric constant, surface conductivity (and microstructural information contained therein, e.g. the $\zeta-$potential), and possibly shape; the results are most promising for oblate particles.

Electroacoustic energy dissipation was described for a dilute suspension. Although the pressure and electric fields interact via the reciprocal relation, energy dissipation results from the independent contributions of each applied field. Viscous dissipation and electrical heating coefficients characterize the $O(c)$ contributions of the suspended particles; typical results were illustrated.

The author is grateful for several valuable conversations with Dr R. W. O'Brien. This work was supported by a grant from the Australian Research Council and a NATO fellowship from the National Science Foundation.

REFERENCES

ALLEGRA, J. R. & HAWLEY, S. A. 1971 Attenuation of sound in suspensions and emulsions: theory and experiments. *J. Acoust. Soc. Am.* **51**, 1545–1564.

BASSET, A. B. 1888 *A Treatise on Hydrodynamics*, vol. 2. Cambridge: Deighton Bell.

BATCHELOR, G. K. 1967 *An Introduction to Fluid Dynamics*. Cambridge University Press.

BOOTH, F. & ENDERBY, J. A. 1952 On electrical effects due to sound waves in colloidal suspension. *Proc. Phys. Soc.* **65**, 321–324.

DEBYE, P. 1933 A method for the determination of the mass of electrolyte ions. *J. Chem. Phys.* **1**, 13–16.

DUKHIN, S. S. & DERJAGUIN, B. V. 1974 *Electrokinetic Phenomena: Surface and Colloid Science*, vol. 7 (ed. E. Matijevic). Wiley.

DUKHIN, S. S. & SHILOV, V. N. 1980 Kinetic aspects of electrochemistry of disperse systems II. Induced dipole moment and the non-equilibrium double-layer of a colloid particle. *Adv. Colloid Interface Sci.* **13**, 153–195.

ENDERBY, J. A. 1951 On electrical effects due to sound waves in colloidal suspensions. *Proc. R. Soc.* A **207**, 329–342.

FRICKE, H. 1953 The Maxwell–Wagner dispersion in a suspension of ellipsoids. *J. Phys. Chem.* **57**, 934–937.

GHADDAR, N. K., MAGEN, M., MIKIC, B. B. & PATERA, A. T. 1986 Numerical investigation of incompressible flow in grooved channels. Part 2. Resonance and oscillatory heat-transfer enhancement. *J. Fluid Mech.* **168**, 541–567.

HARNWELL, G. P. 1949 *Principles of Electricity and Magnetism*. McGraw-Hill.

HERMANS, J. 1938 Charged colloidal particles in an ultrasonic field. *Phil. Mag.* **25**, 426.

HUNTER, R. J. 1987 *Foundations of Colloid Science*, vol. 1. Clarendon.

JACKSON, J. D. 1962 *Classical Electrodynamics*. John Wiley.

KIM, S. & KARRILA, S. J. 1991 *Microhydrodynamics: Principles and Selected Applications*. Butterworth–Heinemann.

LANDAU, L. D., LIFSHITZ, E. M. & PITAEVSKII, L. P. 1984 *Electrodynamics of Continuous Media*. Pergamon.

LAWRENCE, C. J. & WEINBAUM, S. 1988 The unsteady force on a body at low Reynolds number; the axisymmetric motion of a spheroid. *J. Fluid Mech.* **189**, 463–489.

LIGHTHILL, M. J. 1978 *Waves in Fluids*. Cambridge University Press.

LOEWENBERG, M. 1993*a* The unsteady Stokes resistance of arbitrarily oriented, finite-length cylinders. *Phys. Fluids* A **5**, 3004–3006.

LOEWENBERG, M. 1993*b* The Stokes resistance, added mass, and Basset force for arbitrarily oriented, finite-length cylinders. *Phys. Fluids* A **5**, 765–767.

LOEWENBERG, M. 1994*a* Axisymmetric, unsteady Stokes flow past an oscillating, finite-length cylinder. *J. Fluid Mech.* **265**, 265–288.

LOEWENBERG, M. 1994*b* Asymmetric, oscillatory motion of a finite-length cylinder: the macroscopic effect of particle edges. *Phys. Fluids* A **6**, 1095–1107.

LOEWENBERG, M. & O'BRIEN, R. W. 1992 The dynamic mobility of nonspherical particles. *J. Colloid Interface Sci.* **150**, 158–168.

MANGELSDORF, C. S. & WHITE, L. R. 1992 Electrophoretic mobility of a spherical colloidal particle in an oscillating electric field. *J. Chem. Soc. Faraday Trans.* **88**, 3567–3581.

MARLOWE, B. J., FAIRHURST, D. & PENDSE, H. P. 1988 Colloid vibration potential and the electrokinetic characterization of concentrated colloids. *Langmuir* **4**, 611–626.

O'BRIEN, R. W. 1983 The solution of the electrokinetic equations for colloidal particles with thin double layers. *J. Colloid Interface Sci.* **92**, 204–216.

O'BRIEN, R. W. 1986 The high-frequency dielectric dispersion of a colloid. *J. Colloid Interface Sci.* **113**, 81–93.

O'BRIEN, R. W. 1988 Electro-acoustic effects in a dilute suspension of spherical particles. *J. Fluid Mech.* **190**, 71–86.

O'BRIEN, R. W. 1990 The electroacoustic equations for a colloidal suspension. *J. Fluid Mech.* **212**, 81–93.

O'BRIEN, R. W. & ROWLANDS, W. N. 1993 Measuring the surface conductivity of Kaolinite particles. *J. Colloid Interface Sci.* **159**, 471–476.

O'BRIEN, R. W. & WARD, D. N. 1988 The electrophoresis of a spheroid with a thin double layer. *J. Colloid Interface Sci.* **121**, 402–413.

POZRIKIDIS, C. 1989*a* A study of linearized oscillatory flow past particles by the boundary-integral method. *J. Fluid Mech.* **202**, 17–41.

POZRIKIDIS, C. 1989*b* A singularity method for unsteady linearized flow. *Phys. Fluids* A **1**, 1508–1520.

POZRIKIDIS, C. 1992 *Boundary Integral and Singularity Methods.* Cambridge University Press.

RIDER, P. F. & O'BRIEN, R. W. 1993 The dynamic mobility of particles in a non-dilute suspension. *J. Fluid Mech.* **257**, 607–636.

RUSSEL, W. B., SAVILLE, D. A. & SCHOWALTER, W. R. 1989 *Colloidal Dispersions.* Cambridge University Press.

SAWATZKY, R. P. & BABCHIN, A. J. 1993 Hydrodynamics of electrophoretic motion in an alternating electric field. *J. Fluid Mech.* **246**, 321–334.

SMOLUCHOWSKI, M. VON 1903 Contribution à la théorie de l'endosmose électrique et de quelques phenomènes corrélatifs. *Bull. Intl Acad. Sci. Cracovie* **8**, 182–200.

SOBEY, I. J. 1985 Observation of waves during oscillatory channel flow. *J. Fluid Mech.* **151**, 395–426.

STOKES, G. G. 1851 On the effect of internal friction of fluids on the motion of pendulum. *Trans. Camb. Phil. Soc.* **9**, 8.

STRATTON, J. A. 1941 *Electromagnetic Theory.* McGraw-Hill.

TEMKIN, S. 1981 *Elements of Acoustics.* Wiley.